Cement and Concrete Research 90 (2016) 144–161

Contents lists available at ScienceDirect

Cement and Concrete Research

journal homepage: www.elsevier.com/locate/cemconres

Time evolutions of non-aging viscoelastic Poisson's ratio of concrete and implications for creep of C-S-H

Abudushalamu Aili[a], Matthieu Vandamme[b,*], Jean-Michel Torrenti[a], Benoit Masson[c], Julien Sanahuja[d]

[a]Université Paris-Est, IFSTTAR, 14 Boulevard Newton, Champs-sur-Marne F-77420, France
[b]Université Paris-Est, Laboratoire Navier (UMR 8205), CNRS, ENPC, IFSTTAR, Marne-la-Vallée F-77455, France
[c]EDF-DIN-SEPTEN, Division GS - Groupe Enceintes de confinement, 12-14 Avenue Dutriévoz, Villieurbanne F-69628, France
[d]Département Mécanique des Matériaux et des Composants, EDF R&D, Site des Renardières, Avenue des Renardières, Moret-Sur-Loing Cedex 77818, France

ARTICLE INFO

Article history:
Received 26 April 2016
Received in revised form 5 September 2016
Accepted 20 September 2016
Available online 6 October 2016

Keywords:
Concrete (E)
C-S-H (B)
Creep (C)
Poisson's ratio

ABSTRACT

The viscoelastic Poisson's ratio of concrete is an essential parameter to study creep and loss of prestress in biaxially prestressed structures. Here we first aim to scrutinize the various existing definitions of this ratio. We then analyze all creep data of concrete available in literature that make it possible to compute the evolutions of this viscoelastic Poisson's ratio, which, for mature concrete, is found to remain roughly constant or slightly decrease over time, such as to reach a long-term value always comprised between 0.15 and 0.2. Then, the long-term viscoelastic Poisson's ratio of concrete is downscaled to the level of calcium silicate hydrates (noted C-S-H) with micromechanics. The long-term viscoelastic Poisson's ratio of the C-S-H gel is found to range between 0 and 0.2. Finally, the identification of this range is used to discuss various potential creep mechanisms at the level of the C-S-H particles.

1. Introduction

The containment of the typical French nuclear power vessel is a massive concrete structure which is biaxially prestressed and is designed to withstand an internal overpressure of 0.5 MPa in case of accident [1]. To extend the service life of the containment, we need to ensure that the prestress remains sufficient in order to avoid tensile stress and thus limit cracks in the event of such an accident. However, the prestress decreases over time, because of a combination of relaxation of steel and delayed strain of concrete (i.e., creep and shrinkage). Here biaxial creep is considered. In this case, in order to predict the creep of concrete and the resulting loss of prestress, we need to know more than only the 1-dimensional creep behavior of the concrete: we need to know its full 3-dimensional creep behavior. Within the framework of isotropic linear viscoelasticity, this 3-dimensional creep behavior is fully characterized by two creep compliances or relaxation moduli: for instance, on top of the uniaxial creep compliance considered in most models, one can use a viscoelastic (i.e., time-dependent) Poisson's ratio. However, although numerous studies (e.g., [2,3]) and models (e.g., MC10 [4], Eurocode 2 [5], ACI [6]) are devoted to the uniaxial creep compliance, the evolution of the viscoelastic Poisson's ratio of concrete with time has been much less scrutinized.

A first issue when considering a viscoelastic Poisson's ratio is that its definition is not unique [7], even when considering simple uniaxial compression, and in spite of the fact that all authors define it through a ratio of axial strain to lateral strain. For instance, some authors like Neville [8] define it through a ratio of the creep strains only, while others (e.g., [9]) define it through a ratio of the total mechanical strains (which are equal to the sum of the elastic strains and of the creep strains). For what concerns the value of this ratio or its evolution over time, a very large scatter is observed. For instance, with the definition he chose, Neville [8] gathered the following values for the viscoelastic Poisson's ratio: close to 0 [10,11], equal to 0.05 [12,13], equal to the elastic Poisson's ratio [14,15], increasing with time [16], or decreasing with time [17] . A possible reason that could partly explain this large scatter is that the various experiments gathered by Neville were performed under various —and sometimes uncontrolled— hydric conditions. In our present work, we will focus on the evolutions of a viscoelastic Poisson's ratio during basic creep experiments, during which no water is exchanged between sample and environment. Such condition is achieved either by sealing the sample [9,18-21], or by controlling the relative humidity of the envi-

* Corresponding author.
E-mail address: matthieu.vandamme@enpc.fr (M. Vandamme).

http://dx.doi.org/10.1016/j.cemconres.2016.09.014
0008-8846/

ronment to the same relative humidity as that of the sample [22]. As a prerequisite, we will need to clearly define the viscoelastic Poisson's ratio we will consider, and determine how our definition compares with definitions used elsewhere.

For concretes made with ordinary Portland cement paste, there is a consensus that the main phase responsible for the creep of concrete is the calcium silicate hydrates (noted C-S-H) [23]. C-S-H is layered at the nanometric scale —we will refer to stacks of C-S-H layers as to C-S-H 'particles'— and forms a gel at a larger scale. One can reasonably wonder how the viscoelastic Poisson's ratio of concrete is related to the viscoelastic Poisson's ratio of the C-S-H gel and to the creep mechanism of the C-S-H particles. By performing some downscaling, we aim at shedding some light on these relations.

First, we define the viscoelastic Poisson's ratio we will consider in this study and compare it with alternative definitions found in the literature. Secondly, we perform an analysis of basic creep data on concrete from the literature, to determine how this viscoelastic Poisson's ratio evolves with time. Then, by downscaling, we infer the long-term viscoelastic Poisson's ratio of the C-S-H gel. Finally, we consider various creep mechanisms at the scale of the C-S-H particles and assess, by downscaling again, whether those mechanisms are possible or not.

2. Viscoelastic Poisson's ratio for creep studies

This section is devoted to introduce a viscoelastic Poisson's ratio for creep studies. To define it, in Section 2.1 we consider ideal relaxation/creep experiments, i.e., experiments with an instantaneous loading. During an ideal creep experiment, the measured strains (referred to as the 'total' strains) can be separated into an elastic contribution (termed 'elastic' strains) and a delayed one (termed 'creep' strains). Next, we introduce a definition of viscoelastic Poisson's ratio based on total strains: we will use this definition throughout the paper. A detailed introduction of other possible definitions and of their interest can be found in [7]. In Section 2.2, the introduced viscoelastic Poisson's ratio is compared to an alternative definition based on creep strains only. In Section 2.3, we discuss the potential anisotropy of the time-dependent behavior of cementitious materials mentioned by some, and show that the viscoelastic Poisson's ratio we introduced can be considered isotropic.

Concrete is an aging material, i.e., its mechanical properties depend on its age [24,25]. However, mature concrete can reasonably be considered non-aging. Also, up to about at least 40% of its strength, concrete can reasonably be assumed to be linear viscoelastic [8]. In this article, we restrict ourselves to a material that is isotropic linear non-aging viscoelastic. For such a material submitted to infinitesimal strains in isothermal conditions, the time-dependent state equations that link the stress tensor $\underline{\underline{\sigma}}$ (decomposed into the volumetric stress $\sigma_v = \mathrm{tr}(\underline{\underline{\sigma}})/3$ and the deviatoric stress tensor $\underline{\underline{s}}$ such that $\underline{\underline{\sigma}} = \sigma_v \underline{\underline{1}} + \underline{\underline{s}}$, where tr is the trace operator and $\underline{\underline{1}}$ is the unit tensor) to the strain tensor $\underline{\underline{\varepsilon}}$ (decomposed into the volumetric strain $\varepsilon_v = \mathrm{tr}(\underline{\underline{\varepsilon}})$ and the deviatoric strain tensor $\underline{\underline{e}}$ such that $\underline{\underline{\varepsilon}} = (\varepsilon_v/3)\underline{\underline{1}} + \underline{\underline{e}}$) are [26]:

$$\sigma_v(t) = K(t) \otimes \dot{\varepsilon}_v(t) \tag{1a}$$

$$s_{ij}(t) = 2G(t) \otimes \dot{e}_{ij}(t) \tag{1b}$$

where $K(t)$ and $G(t)$ are called the bulk relaxation modulus and the shear relaxation modulus, respectively, $\otimes$ holds for the convolution product defined as $f \otimes g = \int_{-\infty}^{t} f(t-\tau)g(\tau)d\tau$ and $\dot{f}$ holds for the derivative with respect to time such as $\dot{f} = df(t)/dt$. Note that the definition of the convolution product $\otimes$ does not involve any differentiation with respect to time: differentiation with respect to time is indicated explicitly in the right-hand term of the state Eqs. (1a) and (1b), which can equivalently be written [26]:

$$\varepsilon_v(t) = J_K(t) \otimes \dot{\sigma}_v(t) \tag{2a}$$

$$e_{ij}(t) = \frac{1}{2} J_G(t) \otimes \dot{s}_{ij}(t) \tag{2b}$$

where $J_K(t)$ and $J_G(t)$ are called the bulk creep compliance and the shear creep compliance, respectively. Following the denomination of Bažant et al. [27], we name $J_K(t) - J_K(0)$ and $J_G(t) - J_G(0)$ bulk and shear creep functions, respectively.

Starting from the state Eqs. (1a), (1b), (2a) and (2b), in uniaxial testing, we can show that the axial stress history $\sigma_a(t)$ and the axial strain history $\varepsilon_a(t)$ are related by [26]:

$$\sigma_a(t) = E(t) \otimes \dot{\varepsilon}_a(t) \tag{3a}$$

$$\varepsilon_a(t) = J_E(t) \otimes \dot{\sigma}_a(t) \tag{3b}$$

where $E(t)$ and $J_E(t)$ are called the uniaxial relaxation modulus and the uniaxial creep compliance, respectively.

2.1. Definition of viscoelastic Poisson's ratio for isotropic linear non-aging viscoelastic solids

Now, we consider an ideal uniaxial relaxation or an ideal creep experiment, i.e., an experiment in which the displacement or the load, respectively, is applied instantaneously and kept constant over time. Based on those two thought experiments, from the ratio of the radial dilation to the axial contraction, we can define two Poisson's ratios:

$$\nu_r(t) = -\frac{\varepsilon_l(t)}{\varepsilon_a^0} \quad \text{during a uniaxial relaxation experiment for which} \quad \varepsilon_a(t) = \varepsilon_a^0 \tag{4a}$$

$$\nu_c(t) = -\frac{\varepsilon_l(t)}{\varepsilon_a(t)} \quad \text{during a uniaxial creep experiment for which} \quad \sigma_a(t) = \sigma_a^0 \tag{4b}$$

which we termed relaxation Poisson's ratio ν_r and creep Poisson's ratio ν_c. They can be expressed as functions of the bulk and shear time-dependent properties:

$$\hat{\nu}_r(s) = \frac{3\hat{K}(s) - 2\hat{G}(s)}{2s(3\hat{K}(s) + \hat{G}(s))} \tag{5a}$$

$$\nu_c(t) = \frac{3J_G(t) - 2J_K(t)}{2\,(3J_G(t) + J_K(t))} \tag{5b}$$

where s is the Laplace variable and where $\hat{f}(s)$ represents the Laplace transform of the function $f(t)$. Those two Poisson's ratios are related through the uniaxial creep compliance $J_E(t)$ by:

$$\nu_c(t) = \left(\nu_r(t) \otimes \dot{J}_E(t)\right) / J_E(t) \tag{6}$$

Various studies [7,28-31] already discussed the difference between various definitions of Poisson's ratios, including the relaxation Poisson's ratio ν_r and creep Poisson's ratio ν_c. The principle of correspondence [26], which is of great use for solving linear viscoelastic problems analytically, is only applicable to the relaxation Poisson's ratio ν_r, not to the creep Poisson's ratio ν_c [7,28-31]. Said

otherwise, if we want to infer the solution to a linear viscoelastic problem from the solution to the corresponding elastic one, we need to replace the elastic Poisson's ratio by the s-multiplied Laplace transform of the relaxation Poisson's ratio $s\widehat{\nu_r}$, not of the creep Poisson's ratio $s\widehat{\nu_c}$. Therefore, the relaxation Poisson's ratio ν_r is a material property, which can be used to predict the response of the material under a generic load history. In contrast, the correspondence principle cannot be applied to the creep Poisson's ratio ν_c.

In spite of the theoretical differences that exist between the two Poisson's ratios ν_r and ν_c, their initial and asymptotic values are equal, and so are their initial and asymptotic time-derivatives [7]. Moreover, in practice, for all cementitious materials (i.e., cement paste, mortar, or concrete) on which we could analyze biaxial creep data, the difference between those two Poisson's ratios was negligible at all times. Therefore, in the following, we will not distinguish the two Poisson's ratios and will only refer to it as to the viscoelastic Poisson's ratio of the material: we will note it $\nu(t)$. Note however that, for innovative concretes or for immature ones, the fact that the creep and relaxation Poisson's ratios almost coincide is not guaranteed: consequently, even if the creep Poisson's ratio ν_c can easily be obtained with Eq. (7) from creep data, experimentalists should always calculate the relaxation Poisson's ratio ν_r as well (with the above relation via transforms or via a numerical fitting routine), to check if the difference between the two Poisson's ratios is indeed always negligible.

In the rest of the manuscript, the viscoelastic Poisson's ratio of the material will be back-calculated from creep experiments by using Eq. (7) that was derived for the creep Poisson's ratio: we thus retrieve the definition of Eq. (7) that we introduced. When needed, we will also consider that this viscoelastic Poisson's ratio $\nu(t)$ satisfies the elastic-viscoelastic correspondence principle, which can theoretically only be applied to the relaxation Poisson's ratio.

The viscoelastic Poisson's ratio $\nu(t)$ that we will use throughout this work relates strains and stresses for a triaxial creep experiment through:

$$\varepsilon_i(t) = J_E(t)\sigma_i^0 - \left(\sigma_j^0 + \sigma_k^0\right)\nu(t)J_E(t), \quad \text{where} \quad i \neq j \neq k \in \{1,2,3\}, \tag{7}$$

where σ_i^0, σ_j^0, and σ_k^0 are the constant loads instantaneously applied in the principal directions, and $\varepsilon_i(t)$, $\varepsilon_j(t)$, and $\varepsilon_k(t)$ are the strains in those same principal directions. This definition makes it possible to retrieve a definition found elsewhere for uniaxial creep tests [9,18,21]:

$$\nu(t) = -\frac{\varepsilon_2(t)}{\varepsilon_1(t)} = -\frac{\varepsilon_3(t)}{\varepsilon_1(t)} \text{ with a load applied in direction 1 only,} \tag{8}$$

and another definition found elsewhere for biaxial creep tests [9,18,21]:

$$\nu(t) = -\frac{\varepsilon_3(t)}{\varepsilon_1(t) + \varepsilon_2(t) - \varepsilon_3(t)} \text{ with a load applied in directions 1 and 2.} \tag{9}$$

The viscoelastic Poisson's ratio here introduced is defined based on total strains: one cannot calculate it when only the creep strains are reported (as is the case, e.g., in [32,33]), unless the elastic strains can be estimated.

2.2. Definition based on creep strains

One of the most reported Poisson's ratios in the literature is defined based on creep strains [8,13,32,34-39]. For instance, for uniaxial creep tests, Neville [8] defined a uniaxial creep-based Poisson's ratio as:

$$\tilde{\nu}(t) = -\frac{\varepsilon_l(t) - \varepsilon_l^0}{\varepsilon_a(t) - \varepsilon_a^0} \tag{10}$$

where $\varepsilon_l(t)$, $\varepsilon_a(t)$ are the total lateral and axial strain, respectively, and where $\varepsilon_l^0 = \varepsilon_l(0)$ and $\varepsilon_a^0 = \varepsilon_a(0)$ are the lateral and axial elastic strains, respectively. Thus, $\varepsilon_l(t) - \varepsilon_l^0$ and $\varepsilon_a(t) - \varepsilon_a^0$ are the lateral and axial creep strains, respectively. In comparison with the viscoelastic Poisson's ratio $\nu(t)$ that we introduced in Eq. (7), one could draw the following analogy: the creep-based Poisson's ratio corresponds to a creep function, while the viscoelastic Poisson's ratio corresponds to a creep compliance.

The main interest of the creep-based Poisson's ratio $\tilde{\nu}(t)$ is that only creep strains are needed to compute it. Thus, it can be reported for any creep experiment, even in absence of any information on the elastic properties of the material. But this interest is in fact a drawback, which is the same drawback as for any creep function compared with its corresponding creep compliance.

The first drawback is that, if one reports only the creep-based Poisson's ratio, he/she may omit to report the elastic Poisson's ratio. In such case, the creep-based Poisson's ratio becomes quite useless: if one does not keep the load constant after the initial loading, one would be unable to calculate how the ratio between lateral and axial strain would evolve over time. In contrast, such omission is not possible if the viscoelastic Poisson's ratio is reported, since this ratio includes the elastic data: indeed, $\nu(0)$ is the elastic Poisson's ratio.

Creep functions (and hence the creep-based Poisson's ratio) are sensitive to the duration of the loading, which, for any creep test, is never instantaneous. As a consequence, any creep function is associated to an apparent elastic modulus, which must be measured from the strain at the end of the loading phase. Yet, when creep functions are reported in the literature, the associated apparent elastic modulus is not always reported or measured, and, when it is measured, it is sometimes measured from a different test [27]. The error that may arise from such a wrong combination could be nonnegligible.

In conclusions, in the spirit of Bažant et al. [27], who recommended to report creep compliances rather than creep functions, we recommend the use of the viscoelastic Poisson's ratio rather than the creep-based Poisson's ratio. In any case, if one chooses to report the creep-based Poisson's ratio, he/she should report meaningful elastic properties as well.

2.3. Potential anisotropy of time-dependent behavior

A few works [8,22,32] wondered whether the creep-based Poisson's ratio of concrete is anisotropic during a multiaxial creep test. They reached the conclusion that it can be. Here, we discuss their results.

To reach their conclusions, the authors proposed, for triaxial loading, the following definition for a direction-specific creep-based Poisson's ratio $\tilde{\nu}_i$:

$$\varepsilon_i(t) - \varepsilon_i(0) = J_E^{cu}\left(\sigma_i^0 - \tilde{\nu}_i\left(\sigma_j^0 + \sigma_k^0\right)\right) \text{ where } i \neq j \neq k \in \{1,2,3\}. \tag{11}$$

which is a definition based on creep strains. Note that in this definition intervenes the uniaxial creep compliance J_E^{cu}, which is measured from an independent uniaxial creep test in which the

axial load σ_a^0 is equal to the maximum load of the triaxial test (i.e., $\sigma_a^0 = \max_{i\in\{1,2,3\}}\{\sigma_i\}$).

For instance, Gopalakrishnan [22] performed 13 different triaxial tests on a cubic concrete sample. Among these 13 tests, we consider the 11 tests that yielded an elastic Poisson's ratio between 0 and 0.3. His results showed that the direction-specific creep-based Poisson's ratios $\tilde{\nu}_i$ obtained in the three directions $i \in \{1,2,3\}$ differ from each other. However, we believe that this anisotropy is mostly due to the fact that he only took into account creep strains, i.e., that he used uniaxial creep functions instead of uniaxial creep compliances.

Here, we propose an alternative way to analyze their data. This alternative relies on the data from the triaxial experiments only. First, we compute the volumetric strain $\varepsilon_v(t)$ and applied volumetric stress σ_v^0, from which we obtain the volumetric creep compliance $J_K(t) = \varepsilon_v(t)/\sigma_v^0$. Second, we compute the von Mises strain $\varepsilon_d(t) = \sqrt{3J_2^e(t)}$ (where $J_2^e(t)$ is the second invariant of the deviatoric strain tensor e_{ij}) and von Mises stress $\sigma_d^0 = \sqrt{3J_2^{s^0}}$ (where $J_2^{s^0}$ is the second invariant of deviatoric stress tensor s_{ij}), from which we obtain the shear creep compliance $J_G(t) = 2\varepsilon_d(t)/\sigma_d^0$. Then, from the knowledge of the creep compliances $J_K(t)$ and $J_G(t)$, we obtain the uniaxial creep compliance $J_E(t) = J_K(t)/9 + J_G(t)/3$. Finally, by applying Eq. (7) while rotating the indices $i \neq j \neq k \in \{1,2,3\}$, we can obtain, from the triaxial data, 3 directional viscoelastic Poisson's ratios, which we note ν_1, ν_2, and ν_3.

For instance, we consider the test TC10 in [22], in which the specimen is subjected to a triaxial compression: the 3 principal compression stresses are 13.24 MPa, 1.78 MPa and 1.83 MPa. We computed the 3 directional viscoelastic Poisson's ratios as explained above. Our results are displayed in Fig. 1, together with the 3 directional creep-based Poisson's ratio reported by the author of [22]. The maximum difference between the 3 creep-based Poisson's ratios (i.e., $\max_{i\neq j\in\{1,2,3\}}\{\tilde{\nu}_i(t) - \tilde{\nu}_j(t)\}$) displayed in Fig. 1a is 0.14. In contrast, the maximum difference between the 3 directional viscoelastic Poisson's ratios that we introduced (i.e., $\max_{i\neq j\in\{1,2,3\}}\{\nu_i(t) - \nu_j(t)\}$) and that are displayed in Fig. 1b is reduced to 0.019.

In fact, for the 11 tests considered from [22], we computed the 3 directional creep-based Poisson's ratios with Eq. (11) (as did the authors) and the 3 directional creep-based Poisson's ratios with Eq. (7) (see Appendix A). For all 11 tests, the mean value of the maximum difference $\max_{i\neq j\in\{1,2,3\}}\{\tilde{\nu}_i(t) - \tilde{\nu}_j(t)\}$ between the 3 directional creep-based Poisson's ratio was 0.1182 and its standard deviation was 0.1245. In contrast, for the same 11 tests, the mean value of the maximum difference $\max_{i\neq j\in\{1,2,3\}}\{\nu_i(t) - \nu_j(t)\}$ between the 3 directional viscoelastic Poisson's ratios was 0.0367 and its standard deviation was 0.0441.

Therefore, by working with viscoelastic Poisson's ratios rather than creep-based ones, and by consistently analyzing data from a unique test rather than from 2 independent ones, any potential anisotropy of a time-dependent Poisson's ratio vanished. In short: the viscoelastic Poisson's ratio of concrete can be considered as isotropic. Note that this conclusion is fully consistent with the theory of linear viscoelasticity, according to which, for an isotropic solid, the viscoelastic Poisson's ratio should have no reason to exhibit any anisotropy. Such conclusion is only valid for cases for which the load is lower than 30% of the strength, for which neither cracking nor damage is involved.

3. Evolution of viscoelastic Poisson's ratio of concrete

In this section, based on experimental results of basic creep of concrete available in the literature and for which the strains were measured in more than one direction, we analyze how the viscoelastic Poisson's ratio of concrete evolves over time. Here, following the reasoning explained in Section 2.3, we consider only experiments for which both the creep strains and the elastic strains were measured. In these tests, the samples are either sealed [9,18-21] or stored in an environment whose relative humidity is close to the relative humidity inside the sample [22]. For each creep test, a reference specimen is used to measure autogenous shrinkage. This autogenous shrinkage is subtracted from the strain of the loaded specimen to obtain the strain only due to stress, i.e., the basic creep strain. Then, injecting the values of applied stress and stress-induced strains into Eq. (7), the evolution of the viscoelastic Poisson's ratio of the concrete samples with time is back-calculated. The data considered are the following:

- Gopalakrishnan [22] performed triaxial creep tests on a cubic sample made of concrete with one mix design. The samples were always kept in a relative humidity of about 98%. The strain was measured by strain gauges of resolution 10 μm/m, with four strain gauges per surface. The load was applied by four high tensile steel rods whose relaxation was less than 0.2%. The load was provided by a 100-ton hydraulic jack and the load in the jack was indicated by a pressure gauge during the test. The loading age was 8 days.
- Jordaan and Illston [9,18] measured the creep of a cubic sample of concrete with one mix design, under uniaxial and biaxial loads. The samples were coated with one layer of liquid plastic weatherproofing and several coats of resin. The strain was

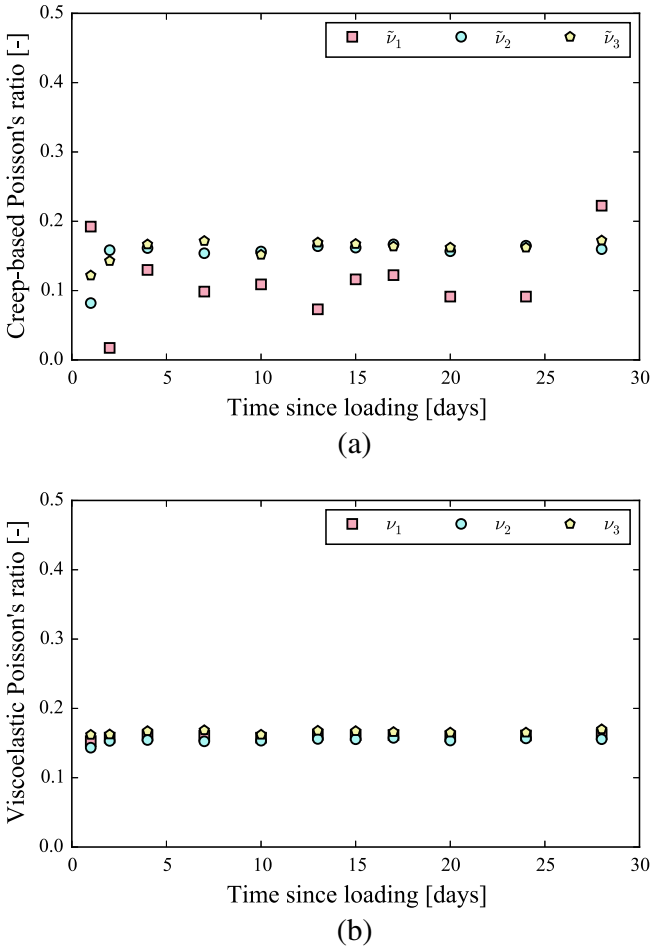

Fig. 1. Dependency of Poisson's ratio on the direction in experiment TC10 in [22]: (a) Creep-based Poisson's ratio reported in [22], calculated from Eq. (11) for three directions; (b) viscoelastic Poisson's ratio calculated from Eq. (7) for three directions.

measured with strain gauges of sensitivity within 1 μm/m. The nominal stress was measured during the test in all three directions. The loading age was 16 days [9] or 7 days [18].

- Kennedy [19] performed uniaxial and triaxial creep tests on cylindrical specimens of concrete with one mix design, but prepared with two types of curing conditions: "AsCast" denotes specimens cured under sealed conditions, while "AirDried" denotes specimens cured at a relative humidity of 50%. Before testing, all samples were coated with two layers of epoxy, then sealed in a copper jacket, placed in a neoprene sleeve and sealed at both ends with neoprene. At the end of each test, the author checked the mass loss of the specimens. The largest mass loss was 0.97% for the sample loaded at the age of 365 days and loaded during 1700 days. The strain was measured with vibrating wire strain gauges embedded in the sample, whose accuracy was 1 μm/m. The load was supplied by a hydraulic pressure which was regulated with a stability of ±5%. A warning system was set to trigger an alarm if a 10% drop in pressure occurred, but the alarm was never triggered during the test.
- Kim et al. [21] prepared cubic samples of concrete with three mix designs (noted C1, C2 and C3) and tested them under uniaxial, biaxial and triaxial loads. The samples were cured under water. Before the test, all exposed faces of the specimens were sealed with a base coat of bituminous sealant and wrapped again in several layers of waterproof plastic film. They stated that they verified the reliability of the sealing method. The strain was measured with embedded gauges of sensitivity 1 μm/m. The load was applied with a spring-loaded creep frame and hydraulic cylinders with loading plates. The hydraulic cylinders were connected to accumulators that automatically compensated for the oil leakage of the cylinders. The authors also stated that they confirmed the effectiveness of their spring-loaded creep frame in providing reliable loads.

All cements that are used for the concretes above are equivalent of cement CEM I clinker in Eurocode. All experimental data are provided in Appendix B.

The results are summarized in Fig. 2a, in which, for each experiment, the evolutions of the viscoelastic Poisson's ratio $\nu(t)$ with time are lumped into: elastic Poisson's ratio ν^0 (i.e., value at loading, displayed on the x-axis), long-term asymptotic viscoelastic Poisson's ratio ν^∞ (which is approximated by the value at the end of the test, displayed on the y-axis), and maximum and minimum viscoelastic Poisson's ratios over time (indicated with the error bars). For almost all experiments, the viscoelastic Poisson's ratio either remained quite constant and equal to its elastic value ν^0 at loading, or decreased continuously toward its long-term value ν^∞.

For each mix design tested, a significant scatter was observed from experiment to experiment. In Fig. 2b, we display, averaged over experiments performed with each mix design, the long-term viscoelastic Poisson's ratio ν^∞ versus the elastic Poisson's ratio ν^0. One can observe that the scatter from test to test was on the order of 0.05, for both the elastic Poisson's ratio and the long-term viscoelastic one. For all concretes tested by Gopalakrishnan [22], Jordaan et al. [9,18], and Kim et al. [21], the elastic ν^0 and long-term viscoelastic ν^∞ Poisson's ratios were almost identical, as a consequence of the fact that, for those concretes, the viscoelastic Poisson's ratio remained almost constant over time. In contrast, for the two concretes tested by Kennedy [19], the final viscoelastic Poisson's ratio ν^∞ was significantly lower than its elastic value ν^0.

From Fig. 2, we observe that, in all cases, the long-term value ν^∞ of the viscoelastic Poisson's ratio was always equal to or smaller than the elastic value ν^0. The variation of viscoelastic Poisson's ratio over time was nonnegligible for certain types of concrete. For all concretes studied here, the long-term value ν^∞ of the viscoelastic Poisson's ratio was comprised between 0.15 and 0.20. So, if the elastic Poisson's ratio of a concrete is in-between 0.15 and 0.20, considering that its viscoelastic Poisson's ratio is constant with time, as proposed by Bažant [2,40], is a very reasonable assumption. We remind the reader that these conclusions are drawn by neglecting aging: they are therefore valid for a mature concrete (for which aging is negligible), but do not hold necessarily for early-age concrete (for which aging is significant).

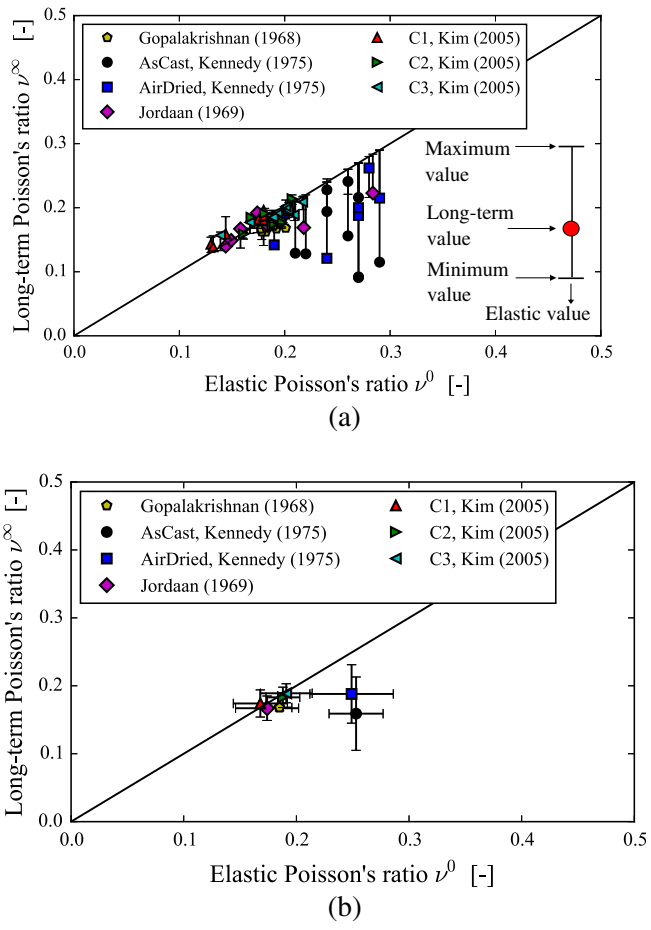

Fig. 2. Creep experiments on concrete [9,19,21,22]: Long-term asymptotic value of the viscoelastic Poisson's ratio versus elastic Poisson's ratio (a) for each individual experiment, and (b) averaged over all experiments performed with one mix design. In subfigure (a), y-axis error bars indicate the maximum and minimum values of the viscoelastic Poisson's ratio during the experiment.

These values of long-term viscoelastic Poisson's ratio ν^∞ of concrete show that the long-term creep of concrete is both deviatoric and volumetric. Indeed, if concrete were to creep only in a deviatoric manner with no asymptote, the long-term viscoelastic Poisson's ratio should theoretically converge toward $\nu^\infty = 0.5$ for infinite times (see Section 4), and hence should at least, in practice, increase with time. However, the experiments here analyzed show that the viscoelastic Poisson's ratio remained constant or decreased slightly with time. Moreover, Fig. 3 highlights the fact that the long-term creep is not only deviatoric but also volumetric: out of the five tests plotted in Fig. 3, four showed an increasing volumetric strain, three of which evolved logarithmically with time during the creep experiment.

4. Downscaling the long-term viscoelastic Poisson's ratio

Knowing the long-term value of the viscoelastic Poisson's ratio of concrete, a back-calculation of the long-term value of the viscoelastic

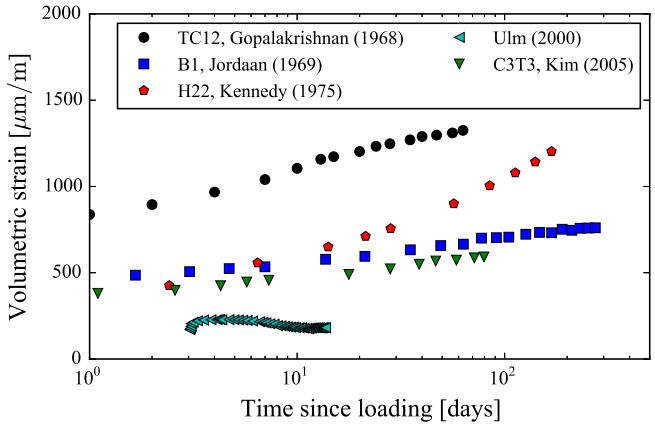

Fig. 3. Evolution of volumetric strain during creep experiment on concrete. Original data are from [9,19-22].

Poisson's ratio of the C-S-H gel is possible. As we shall see, from the knowledge of this long-term viscoelastic Poisson's ratio, some physical conclusions can be inferred. Working with data on cement paste may have been more relevant, but we are aware of only one experimental data on cement paste that we could use [41]. Therefore, in this section, an analysis of data on concrete is presented.

The elastic-viscoelastic correspondence principle [26] is a tool that can transform a linear non-aging viscoelastic problem into a corresponding linear elastic problem. This principle consists in eliminating the explicit time-dependence of the viscoelastic problem by replacing all time-dependent moduli by the s-multiplied Laplace transform (also called Carson transform) of their viscoelastic operator, thus yielding a corresponding elasticity problem in the Laplace domain. Using this principle makes it possible to tackle upscaling of viscoelastic creep compliances, by using corresponding elastic homogenization schemes in the Laplace domain.

Resulting relations in the Laplace domain need to be transformed back into the real time domain, which always remains hard to do analytically, because only a few types of functions can be transformed analytically from the Laplace domain back into the time domain. Nevertheless, one can use the final value theorem [42] to find a relation between the long-term asymptotic values K^∞ and G^∞ of the relaxation moduli, J_K^∞ and J_G^∞ of the creep compliances, and ν^∞ of the viscoelastic Poisson's ratio. For instance, applying the final value theorem [42] to Eq. (5a), we find the following relation between the long-term value ν^∞ of the viscoelastic Poisson's ratio and the long-term bulk K^∞ and shear G^∞ moduli:

$$\lim_{s\to 0}\left(s\hat{\nu}(s)\right)=\lim_{s\to 0}\left(\frac{3\hat{K}-2\hat{G}}{6\hat{K}+2\hat{G}}\frac{s}{s}\right)=\frac{3K^\infty-2G^\infty}{6K^\infty+2G^\infty}=\nu^\infty \tag{12}$$

From this relation, we infer that, if the material creeps with no asymptote in time (which seems to be the case for most cementitious materials [3,43-45], see also Fig. 3), but in a deviatoric manner only (in which case $K^\infty \gg G^\infty$), the viscoelastic Poisson's ratio must converge toward $\nu^\infty = 0.5$. In contrast, if the material creeps with no asymptote in time but in a volumetric manner only (in which case $K^\infty \ll G^\infty$), the viscoelastic Poisson's ratio must converge toward $\nu^\infty = -1$.

In the experiments discussed in Section 3, the duration of the experiments is finite and the viscoelastic Poisson's ratio may not have reached its asymptotic value fully. However, as the viscoelastic Poisson's ratio $\nu(t)$ does not vary much with time, we will consider its value at the end of the experiment as its asymptotic value ν^∞. Based on this approach, we will perform downscaling of the long-term asymptotic viscoelastic Poisson's ratio by using the elastic-viscoelastic correspondence principle and the final value theorem. Note that, although aging is neglected in the downscaling here performed, a micromechanical analysis of the Poisson's ratio that explicitly takes into account aging (which would be needed for early-age materials) is possible [46].

To infer the long-term asymptotic value of the viscoelastic Poisson's ratio of the C-S-H gel from that of the concrete, the concrete is regarded as a multiscale composite material at four different scales, which are displayed in Fig. 4:

- At the largest scale of concrete (see Fig. 4a), the aggregates are considered as spherical inclusions that do not creep and are embedded into a matrix made of cement paste, which creeps.
- At a scale below, i.e., at the scale of the cement paste (see Fig. 4b), portlandite, calcium sulfoaluminates hydrates and the unhydrated clinker are considered as spherical inclusions that do not creep and are embedded into a matrix made of a mixture of C-S-H with capillary pores. This mixture is considered to creep.
- At another scale below (see Fig. 4c), the mixture of C-S-H with capillary pores is considered to be a matrix of C-S-H gel (that contains the gel porosity) that surrounds spherical capillary pores.

We downscaled then the Poisson's ratio from the scale of concrete (Fig. 4a) to the scale of C-S-H gel (Fig. 4c). As a prerequisite to the downscaling, we derive some theoretical results. It should be noted that we do not take into account any interfacial transition zone (ITZ) in this stage of downscaling but the effect of ITZ will be discussed in Section 5.1. In Section 4.1, we derive what the long-term viscoelastic Poisson's ratio is for a composite material made of a matrix that

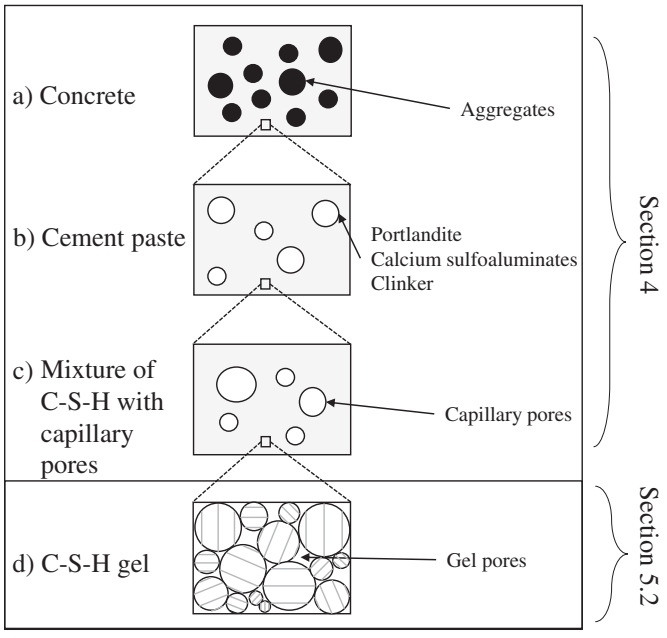

Fig. 4. Multiscale structure of concrete: (a) Concrete as a matrix of cement paste embedding aggregates, (b) cement paste as portlandite, calcium sulfoaluminates hydrates and unhydrated clinker embedded into a matrix made of a mixture of C-S-H with capillary pores, (c) mixture of C-S-H with capillary pores as a matrix of C-S-H gel surrounding capillary porosity, and (d) C-S-H gel as a mixture of C-S-H particles and gel pores. The scales (a), (b) and (c) are considered in Section 4 for the downscaling of the long-term Poisson's ratio, while the scale (d) is considered in Section 5.2 for the analysis of the long-term creep mechanism of C-S-H gel.

creeps and that embeds spherical inclusions that do not creep. In Section 4.2, we derive what the long-term viscoelastic Poisson's ratio is for a composite material made of a matrix that creeps and that surrounds spherical pores.

4.1. Viscoelastic Poisson's ratio of composite made of matrix embedding non-creeping inclusions

Here we consider a composite made of a matrix that embeds spherical inclusions. The matrix is considered to creep, and the inclusions are considered not to creep. The aim is to derive the relation between the long-term value ν_{com}^{∞} of the viscoelastic Poisson's ratio of the composite, the long-term value ν_{m}^{∞} of the viscoelastic Poisson's ratio of the matrix, and the volume fraction f_i of the inclusions.

For such a microstructure, the Mori-Tanaka scheme has been argued to be applicable, for any volume fraction of inclusions [47–49]. So, we apply this scheme to calculate the properties of the composite as a function of the properties of its individual phases . The interface between inclusion and matrix is considered to be perfectly adhesive. Applying the correspondence principle to the elastic Mori-Tanaka homogenization scheme, one finds, in the Laplace domain, the solution to the viscoelastic homogenization problem of interest. Applying the final value theorem [42] to this relation, we obtain a relation between the long-term values K_{com}^{∞} and G_{com}^{∞} of the relaxation moduli of the composite, K_{m}^{∞} and G_{m}^{∞} of the relaxation moduli of the matrix, and K_{i}^{∞} and G_{i}^{∞} of the relaxation moduli of the inclusions:

$$K_{com}^{\infty} = K_{m}^{\infty}\frac{(1-f)\left(K_{m}^{\infty}+\alpha\left(K_{i}^{\infty}-K_{m}^{\infty}\right)\right)+fK_{i}^{\infty}}{(1-f)\left(K_{m}^{\infty}+\alpha\left(K_{i}^{\infty}-K_{m}^{\infty}\right)\right)+fK_{m}^{\infty}} \tag{13a}$$

$$G_{com}^{\infty} = G_{m}^{\infty}\frac{(1-f)\left(G_{m}^{\infty}+\beta\left(G_{i}^{\infty}-G_{m}^{\infty}\right)\right)+fG_{i}^{\infty}}{(1-f)\left(G_{m}^{\infty}+\beta\left(G_{i}^{\infty}-G_{m}^{\infty}\right)\right)+fG_{m}^{\infty}} \tag{13b}$$

where $\alpha = (3K_{m}^{\infty})/(3K_{m}^{\infty}+4G_{m}^{\infty})$ and $\beta = (6K_{m}^{\infty}+12G_{m}^{\infty})/(15K_{m}^{\infty}+20G_{m}^{\infty})$. Then, injecting the relaxation moduli K_{com}^{∞} and G_{com}^{∞} into Eq. (12), we get the expression of the long-term value ν_{com}^{∞} of the viscoelastic Poisson's ratio of the composite. Supposing that the long-term volumetric and deviatoric creep functions of the matrix are non-asymptotic, we let $K_{m}^{\infty}/K_{i}^{\infty} \to 0$ and $G_{m}^{\infty}/G_{i}^{\infty} \to 0$ in the expression of ν_{com}^{∞} and obtain:

$$\nu_{com}^{\infty} = \frac{(10(\nu_{m}^{\infty})^2 - 11(\nu_{m}^{\infty})+3)f + (8(\nu_{m}^{\infty}) - 10(\nu_{m}^{\infty})^2)}{(30(\nu_{m}^{\infty})^2 - 41\nu_{m}^{\infty}+13)f + (8-10\nu_{m}^{\infty})} \tag{14}$$

This equation indicates that the long-term viscoelastic Poisson's ratio of such a composite depends only on the long-term viscoelastic Poisson's ratio of the matrix and on the volume fraction of the inclusions. The relation between the long-term viscoelastic Poisson's ratio ν_{com}^{∞} of the composite and ν_{m}^{∞} of the matrix is displayed in Fig. 5a for various volume fractions f of inclusion.

Fig. 5a shows that if the matrix creeps only deviatorically (i.e., $\nu_{m}^{\infty} = 0.5$) at large times, then the composite must also creep deviatorically only. As the basic creep of concrete is non-asymptotic [50,51] and its long-term viscoelastic Poisson's ratio is strictly lower than 0.5 (see Fig. 2), we can consider that the cement paste creeps not only deviatorically but also volumetrically with no asymptote. Thus, the homogenization scheme developed in this section can be applied to downscale results from the scale of concrete to the scale of the cement paste and to the scale of the mixture of C-S-H with capillary porosity (see Fig. 4).

4.2. Viscoelastic Poisson's ratio of porous medium

Here we consider a composite made of a homogeneous matrix that embeds spherical pores. The aim is to relate the long-term viscoelastic Poisson's ratio ν_{com}^{∞} of the composite to the long-term viscoelastic Poisson's ratio ν_{m}^{∞} of the matrix and the volume fraction ϕ of pores (i.e. porosity).

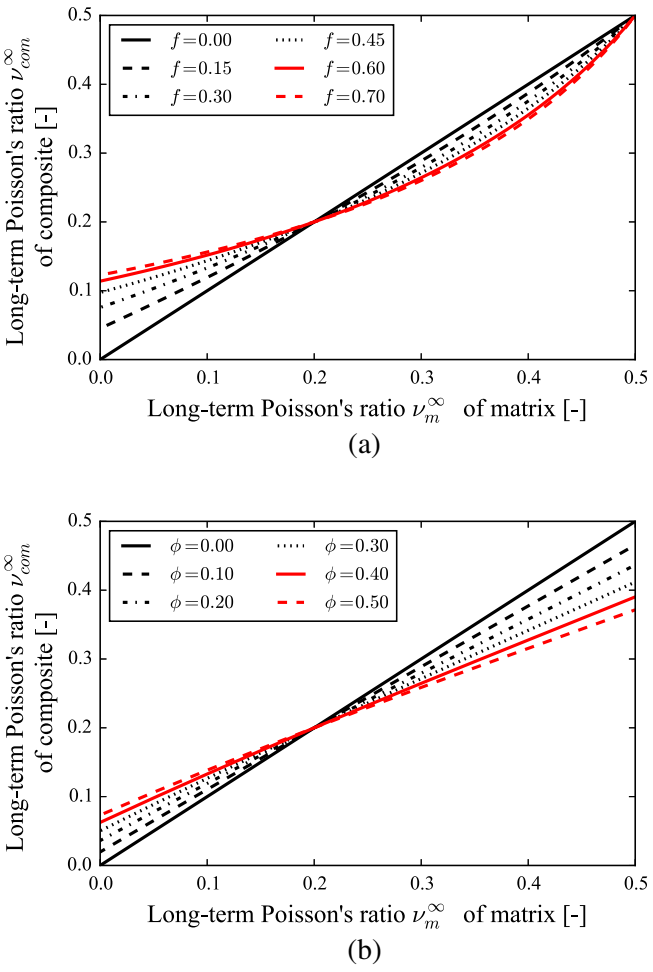

Fig. 5. (a) Long-term viscoelastic Poisson's ratio of a composite made of a creeping matrix that surrounds non-creeping spherical inclusions. f is the volume fraction of inclusions. (b) Long-term viscoelastic Poisson's ratio of a composite made of a creeping matrix that surrounds spherical pores. ϕ is the volume fraction of pores.

Given the microstructure, we apply the Mori-Tanaka scheme to compute the properties of the composite as a function of the properties of its individual phases. Since the homogenization scheme is the same as that used in Section 4.1, the long-term relaxation moduli K_{com}^{∞} and G_{com}^{∞} of the composite read as in Eqs. (13a) and (13b). In this equation, taking into account the fact that $K_{i}^{\infty} = 0$ and $G_{i}^{\infty} = 0$ and injecting them into Eq. (12) yields:

$$\nu_{com}^{\infty} = \frac{(5(\nu_{m}^{\infty})^2 + 2\nu_{m}^{\infty} - 3)\phi + \nu_{m}^{\infty}(10\nu_{m}^{\infty} - 14)}{(15(\nu_{m}^{\infty})^2 + 2\nu_{m}^{\infty} - 13)\phi + (10\nu_{m} - 14)} \tag{15}$$

This equation indicates that the long-term viscoelastic Poisson's ratio of such a composite depends only on the long-term viscoelastic Poisson's ratio of the matrix and on the volume fraction of the pores. The relation between the long-term viscoelastic Poisson's ratios ν_{com}^{∞} of the composite and ν_{m}^{∞} of the matrix is displayed in Fig. 5b for various values of volume fraction of pores. This figure shows that if the matrix creeps only deviatorically (i.e., $\nu_{m}^{\infty} = 0.5$) at large times, the porous medium may creep not only deviatorically, but also volumetrically. It is worth to keep in mind that a pure deviatoric creep at microscopic level does not imply always a pure deviatoric creep at macroscopic level.

4.3. Long-term viscoelastic Poisson's ratio: from concrete down to C-S-H gel

The long-term viscoelastic Poisson's ratio ν_{gel}^{∞} of the C-S-H gel is computed from the results obtained at the scale of concrete by downscaling in three steps, by using the intermediate scales of the cement paste and of the mixture of C-S-H with the capillary porosity (see Fig. 4).

To downscale results from the scale of concrete to the scale of cement paste, we apply the viscoelastic homogenization scheme introduced in Section 4.1. We use Eq. (14), in which the long-term viscoelastic Poisson's ratio used is that of concrete, which is displayed in Fig. 2a, and in which the volume fraction of aggregates is computed from the mix design (see Table 1). Thus, we back-calculate the long-term viscoelastic Poisson's ratio of the cement paste, which plays the role of the matrix in this step of downscaling (see Fig. 4a).

To downscale results from the scale of cement paste to the scale of the mixture of C-S-H with capillary porosity, we apply the viscoelastic homogenization scheme introduced in Section 4.1 again. The volume fraction of each phase is computed by using Powers' model [52], which considers that the volume of cement paste is composed of bulk hydrates (i.e., solid hydrates plus gel pores), unhydrated clinker, and capillary pores. The sample is considered to be fully hydrated if the water-to-cement mass ratio w/c is superior to 0.38 for samples cured under water, and superior to 0.44 for samples cured under sealed conditions [52]. Otherwise, the long-term hydration degree α^{∞} is taken to be equal to $(w/c)/0.38$ for samples cured under water, and to $(w/c)/0.44$ for samples cured under sealed conditions [52]. The volume fraction of bulk hydrates per unit volume of cement paste is $2.12(1-p)\alpha^{\infty}$, where $p = (w/c)/(w/c + \rho_w/\rho_c)$ and where ρ_w and ρ_c are the densities of water and of the clinker grains, respectively. The volume fraction of portlandite per unit volume of bulk hydrates is estimated to be equal to 25%, which is a typical value for CEM I cement pastes [23], from which the volume fraction f_{CH} of portlandite per unit volume of cement paste is $f_{\mathrm{CH}} = 0.53(1-p)\alpha^{\infty}$. The volume fraction of calcium sulfoaluminates hydrates per unit volume of bulk hydrates is estimated to be equal to 15% [23], from which the volume fraction f_{alu} of sulfoaluminates hydrates per unit volume of cement paste is $f_{alu} = 0.32(1-p)\alpha^{\infty}$. The volume fraction f_{cl} of unhydrated clinker per unit volume of cement paste is estimated also with Powers' model [52] to be equal to $f_{cl} = (1-p)(1-\alpha^{\infty})$. Therefore, to downscale results from the scale of cement paste to the scale of the mixture of C-S-H with capillary porosity, we use Eq. (14) by considering that the volume fraction of inclusions is $f_{\mathrm{CH}} + f_{alu} + f_{cl}$. Thus, we back-calculate the long-term viscoelastic Poisson's ratio of the mixture of C-S-H with the capillary porosity, which plays the role of the matrix in this step of downscaling (see Fig. 4b).

To downscale results from the scale of the mixture of C-S-H with the capillary porosity to the scale of the C-S-H gel, we apply the viscoelastic homogenization scheme introduced in Section 4.2. The volume fraction V_{cp} of capillary pores per unit volume of cement paste is estimated with Powers' law [52] as $V_{cp} = p - 1.12(1-p)\alpha^{\infty}$. We use Eq. (15) by considering that the porosity $\phi = V_{cp}/(1 - V_{\mathrm{CH}} - V_{alu} - V_{cl})$ is the volume fraction of capillary pores in the mixture. Thus, we back-calculate the long-term viscoelastic Poisson's ratio of the C-S-H gel, which plays the role of the matrix in this step of downscaling (see Fig. 4c).

Fig. 6 displays the results of this downscaling. The long-term viscoelastic Poisson's ratio ν_{gel}^{∞} of the C-S-H gel is comprised between −0.07 and 0.16, while the long-term viscoelastic Poisson's ratio ν_{c}^{∞} of concrete is comprised between 0.16 and 0.19. As a result of the fact that the slope of the curves displayed in Fig. 5a and b is lower than 1 for Poisson's ratios around 0.2, the long-term viscoelastic Poisson's ratio of C-S-H is more scattered than that of concrete, which indicates that the long-term viscoelastic Poisson's ratio of concrete is rather independent of that of C-S-H gel: the long-term viscoelastic Poisson's ratio of C-S-H has little influence on the long-term viscoelastic Poisson's ratio of concrete. The fact that the estimation of the Poisson's ratio of C-S-H gel is scattered is due to the scatter of the measurement at the level of the concrete.

Even when taking into account the scatter, for all materials considered, the sum of the long-term viscoelastic Poisson's ratio ν_{gel}^{∞} of the C-S-H gel and of its standard deviation is found to be between −0.38 and 0.24, which is significantly smaller than 0.5 and significantly greater than −1. Therefore, given the fact that the creep of cementitious materials is known to exhibit no asymptote [50,51], we infer that the long-term creep of the C-S-H gel is neither deviatoric only (in which case we would observe $\nu_{gel}^{\infty} = 0.5$), nor volumetric only (in which case we would observe $\nu_{gel}^{\infty} = -1$): in the long term, the C-S-H gel creeps both volumetrically and deviatorically.

5. Discussion

5.1. Influence of the interface

The homogenization scheme introduced in Section 4.1 was derived by considering that the interface between inclusion and matrix is perfectly adhesive. Said otherwise, by using this scheme, we considered that there is no discontinuity of displacement, neither at the interface between aggregates and cement paste (see Fig. 4a), nor at the interface between portlandite, calcium sulfoaluminates hydrates, clinker and the mixture of C-S-H with capillary porosity (see Fig. 4b). In practice, adhesion at those two interfaces may not be perfect. The objective of this section is to quantify how this imperfection could alter the findings obtained in Section 4.3.

As was done in Section 4.3, we consider a composite made of a matrix that creeps and surrounds spherical inclusions that do not creep, but we now consider that the interface between matrix and inclusion can be imperfect: a tangential stiffness $K_t(t)$ of the interface is introduced, with a long-term asymptotic value $\lim_{t\to+\infty} K_t(t) = K_t^{\infty}$. The normal displacement at the interface is considered to be

Table 1
Concrete formulation data used for the downscaling of viscoelastic Poisson's ratio. The volume fraction of aggregates is expressed per unit volume of concrete. The volume fraction of portlandite, calcium sulfoaluminates hydrates and unhydrated clinker is expressed per unit volume of cement paste. The volume fraction of capillary pores is expressed per unit volume of mixture of C-S-H with capillary pores.

Concrete	Cement type	Water-to-cement mass ratio	Volume fraction of aggregates	Volume fraction of portlandite, calcium sulfoaluminates hydrates and clinker	Volume fraction of capillary pores Volume fraction of capillary pores
Gopalakrishnan	Type III	0.72	0.725	0.259	0.474
AsCast, Kennedy	Type II	0.425	0.637	0.365	0.173
AirDried, Kennedy	Type II	0.425	0.637	0.365	0.173
Jordaan and Illston	Ordinary Portland cement	0.40	0.641	0.381	0.173
C1, Kim et al.	Type I	0.58	0.715	0.300	0.357
C2, Kim et al.	Type I	0.4	0.7	0.375	0.099
C3, Kim et al.	Type I	0.32	0.691	0.434	0.057

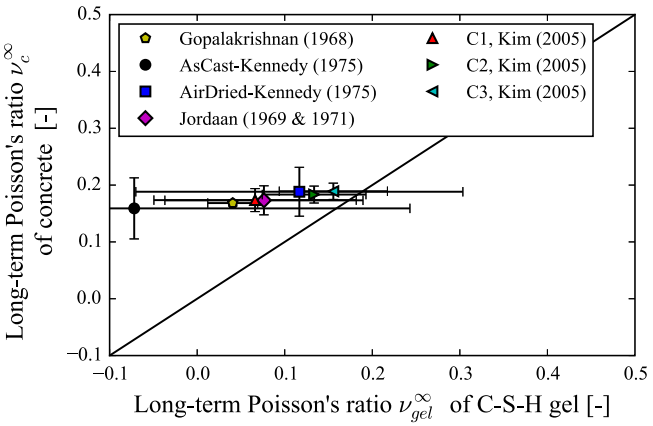

Fig. 6. Long-term viscoelastic Poisson's ratio ν_c^∞ of concrete versus long-term viscoelastic Poisson's ratio ν_{gel}^∞ of C-S-H gel.

continuous, i.e., there is no separation at the interface. The radius of the inclusions is noted R_i. The viscoelastic homogenization scheme is based on the equivalent inclusion method developed by Duan et al. [53] for elastic solids. In his model, the imperfection of the interface is characterized by the dimensionless parameter $m_\theta = K_t R_i / G_m$, where G_m is the shear modulus of the matrix. Using the correspondence principle, the viscoelastic homogenization scheme with imperfect interfaces is derived in the Laplace domain by replacing all elastic parameters in Duan's scheme by the s-multiplied Laplace transform of their corresponding viscoelastic parameter. Then, using again the final value theorem [42], we derive a relation between the long-term viscoelastic Poisson's ratio ν_{com}^∞ of the composite, ν_m^∞ of the matrix, the long-term interface property $m_\theta^\infty = \lim_{t\to+\infty}(K_t(t)R_i/G_m(t))$, and the volume fraction f of inclusions:

$$\nu_{com}^\infty = \frac{A_1(\nu_m^\infty)^2 + B_1\nu_m^\infty + C_1}{A_2(\nu_m^\infty)^2 + B_2\nu_m^\infty + C_2} \tag{16}$$

where the coefficients are:

- $A_1 = 10f^2 m_\theta^\infty + 20f^2 - 20fm_\theta^\infty - 76f + 10m_\theta^\infty + 38$
- $B_1 = -11f^2 m_\theta^\infty - 22f^2 + 19fm_\theta^\infty + 92f - 8m_\theta^\infty - 34$
- $C_1 = 3f^2 m_\theta^\infty + 6f^2 - 3fm_\theta^\infty - 24f$
- $A_2 = 30f^2 m_\theta^\infty + 60f^2 - 30fm_\theta^\infty - 96f$
- $B_2 = -41f^2 m_\theta^\infty - 82f^2 + 31fm_\theta^\infty + 116f + 10m_\theta^\infty + 38$
- $C_2 = 13f^2 m_\theta^\infty + 26f^2 - 5fm_\theta^\infty - 28f - 8m_\theta^\infty - 34$

In the above equation, letting the interface parameter m_θ^∞ tend toward $+\infty$, we retrieve Eq. (14), which is valid for perfectly adhesive interfaces. In contrast, letting the interface parameter m_θ^∞ tend toward 0, we obtain a relation valid in the case of perfectly smooth interfaces. We checked that the relation obtained in this latter case is consistent with the Poisson's ratio obtained by using the elastic homogenization scheme for perfectly smooth interface developed in [54]. Next, we study the influence of the interface conditions on the results when performing a homogenization 1) from the scale of the cement paste to that of the concrete, and 2) from the scale of the C-S-H gel to that of the cement paste.

For what concerns homogenization from the scale of cement paste to the scale of concrete, the interface that plays a role is that between aggregates and cement paste (see Fig. 4a). Here, in accordance with the experimental results of Parrott [41], we consider a concrete made of aggregates at a typical volume fraction of 0.7 and of a cement paste with a long-term viscoelastic Poisson's ratio equal to 0.19. Using Eq. (16), we compute the long-term viscoelastic Poisson's ratio of the concrete as a function of the interface parameter m_θ^∞. The results are displayed in Fig. 7a: to retrieve a long-term viscoelastic Poisson's ratio between 0.15 and 0.2 for concrete (as is observed experimentally, see Fig. 2), Fig. 7a suggests that the interface between aggregates and cement paste can be considered to be perfectly adhesive.

For what concerns homogenization from the scale of the C-S-H gel to the scale of the cement paste, the interfaces that play a role are those between portlandite, calcium sulfoaluminates hydrates, clinker and the mixture of C-S-H with the capillary porosity (see Fig. 4b). Here, in accordance again with the experimental results of Parrott [41], we consider a cement paste with a long-term viscoelastic Poisson's ratio equal to 0.19. This long-term viscoelastic Poisson's ratio is downscaled down to the scale of the C-S-H gel in two steps, to obtain the long-term viscoelastic Poisson's ratio of the C-S-H gel (see Fig. 4b and c). For the first step, we consider the volume fraction of portlandite, calcium sulfoaluminates hydrates and clinker equal to 0.35 (which is the mean value of the volume fractions of portlandite, calcium sulfoaluminates hydrates and clinker in Table 1) and use Eq. (16) to back-calculate the long-term viscoelastic Poisson's ratio of the mixture of C-S-H with capillary porosity, as a function of the parameter m_θ^∞ of its interface with portlandite, calcium sulfoaluminates hydrates and clinker. Then, considering the volume fraction of capillary pores equal to 0.21 (which is the mean value of the volume fractions of capillary pores in Table 1) and using Eq. (15), by

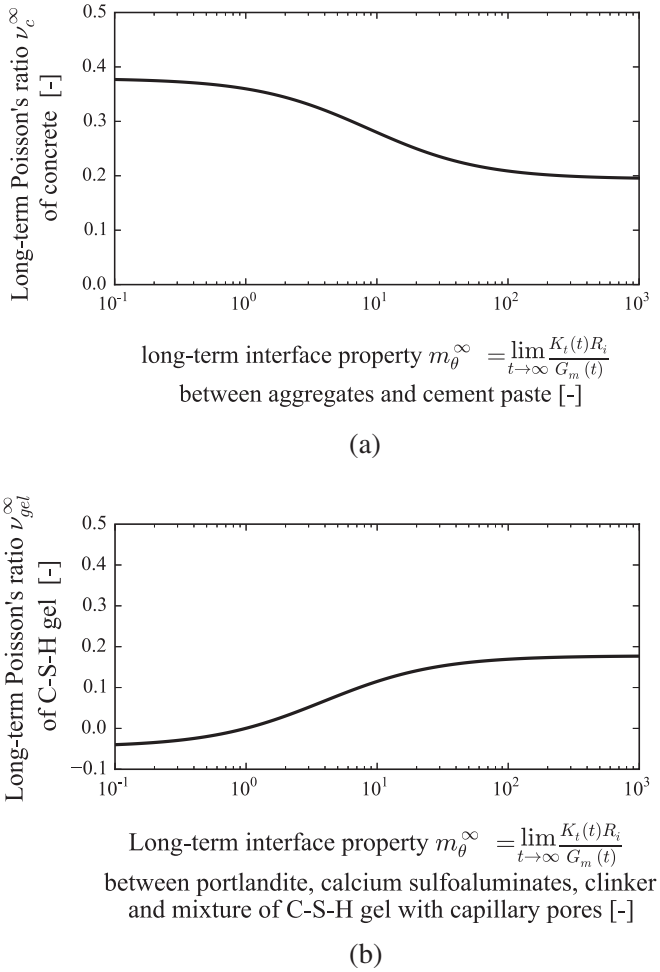

Fig. 7. (a) Upscaled long-term viscoelastic Poisson's ratio of concrete as a function of the property of the interface between aggregates and cement paste. (b) Downscaled long-term viscoelastic Poisson's ratio of C-S-H gel as a function of the property of the interface between portlandite, calcium sulfoaluminates hydrates and clinker on one hand, and the mixture of C-S-H with capillary pores on the other hand.

downscaling we infer the long-term viscoelastic Poisson's ratio ν_{gel}^{∞} of the C-S-H gel. The results are displayed in Fig. 7b: the range over which the long-term viscoelastic Poisson's ratio ν_{gel}^{∞} of the C-S-H gel is almost the same as the scatter of the downscaled value, which is visible in Fig. 6. Said otherwise: the properties of the interface between portlandite, calcium sulfoaluminates hydrates and clinker on one hand, and the mixture of C-S-H with capillary porosity on the other hand, play a negligible role on the back-calculated value of the long-term viscoelastic Poisson's ratio of the C-S-H gel.

From the calculations performed above, we conclude that 1) the interface between aggregates and cement paste can be considered to be perfectly adhesive, and 2) the interface between portlandite, calcium sulfoaluminates hydrates and clinker on one hand, and the mixture of C-S-H with capillary porosity on the other hand, has little influence on the back-calculated long-term viscoelastic Poisson's ratio of the C-S-H gel. It should be noted that such conclusion is only valid for the long-term values of Poisson's ratio. As to whether the interface effect can be neglected or not for the whole time-evolution of Poisson's ratio, no information can be obtained from the above study.

5.2. Implications for creep mechanism of C-S-H gel at large times

Based on the back-calculated long-term viscoelastic Poisson's ratio of the C-S-H gel, which is found to lie between 0 and 0.18 (see Section 4.3), we aim at inferring some implications for the creep mechanism of the C-S-H gel. In the spirit of the model proposed by Jennings et al. [55,56], we consider the C-S-H gel to be made of nanometer-sized C-S-H particles. Two potential creep mechanisms are considered next: long-term creep of the C-S-H gel is due to 1) creep of the C-S-H particles themselves, or 2) creep of the contact points between neighboring C-S-H particles. Note that those conclusions which will be drawn only hold if we consider that the experimental data at the concrete scale are sufficiently reliable.

5.2.1. Creep of C-S-H gel originating from creep of C-S-H particles

In this section, we consider that creep of the C-S-H gel originates from the creep of the C-S-H particles themselves, and that those particles are perfectly bonded to each other. We adopted the model proposed by Tennis and Jennings [55,57] for the description of the microstructure of the C-S-H gel. The C-S-H gel is composed of individual globules of C-S-H particles, which are stacks of C-S-H layers. The globules form zones of Low Density (LD) C-S-H and zones of High Density (HD) C-S-H, whose gel porosity (volume of gel pores over the sum of the volume of solid hydrates and gel pores) is 0.37 and 0.24, respectively [57]. We consider that each globule of C-S-H particle can creep by having its C-S-H layers sliding over each other (see Fig. 8a): the shear relaxation modulus associated to this sliding is noted $G_{CSH}(t)$. In addition, we consider that the distance between solid C-S-H layers could vary over time: the uniaxial relaxation modulus associated to this type of deformation is noted $E_{CSH}(t)$. At large times, the shear and uniaxial relaxation moduli tend toward G_{CSH}^{∞} and E_{CSH}^{∞}, respectively.

Sanahuja [58] developed an elastic homogenization scheme for a composite material made of an assembly of transverse isotropic particles randomly oriented, intermixed with spherical pores. He considered both spherical and aspherical particles. Here we extend his scheme to homogenization of the long-term viscoelastic behavior, again by using the correspondence principle and the final value theorem [42]. Thus, we obtain a relationship between long-term viscoelastic Poisson's ratio ν_{gel}^{∞} of the C-S-H gel and long-term shear relaxation modulus G_{CSH}^{∞} and uniaxial relaxation modulus E_{CSH}^{∞} of the C-S-H particles.

For spherical C-S-H particles, we found that the long-term viscoelastic Poisson's ratio ν_{gel}^{∞} of the C-S-H gel did not depend much on the gel porosity, in the range of its two extreme values, i.e., 0.24 and 0.37. We display this long-term viscoelastic Poisson's ratio ν_{gel}^{∞} of the C-S-H gel in Fig. 9a, as a function of the ratio $G_{CSH}^{\infty}/E_{CSH}^{\infty}$, for a gel porosity of 0.28. If the ratio $G_{CSH}^{\infty}/E_{CSH}^{\infty}$ is equal to 0, i.e., if in the long term C-S-H layers can only slide over each other, the long-term viscoelastic Poisson's ratio of the C-S-H gel must be equal to $\nu_{gel}^{\infty} = 0.40$, which is not consistent with the experimental results obtained by downscaling and displayed in Fig. 6. In contrast, to retrieve the long-term viscoelastic Poisson's ratio ν_{gel}^{∞} of the C-S-H gel observed experimentally, which is between −0.07 and 0.16 (see Fig. 6), and if we still consider spherical C-S-H particles, in the long term both sliding of its C-S-H layers over each other and variations of the interlayer distance must occur.

For oblate C-S-H particles with still a gel porosity equal to 0.28, Fig. 9a displays the long-term viscoelastic Poisson's ratio of the C-S-H gel, as a function of the ratio $G_{CSH}^{\infty}/E_{CSH}^{\infty}$, for two aspect ratio: $r_s = 0.12$ [48] and $r_s = 0.033$ [48]. We observe that, in such case, one can retrieve the long-term creep Poisson's ratio of the C-S-H gel observed experimentally, if $G_{CSH}^{\infty}/E_{CSH}^{\infty} = 0$, i.e., if the C-S-H layers are only allowed to slide over each other, with no variation of the interlayer distance.

In conclusion, if creep of the C-S-H gel is due to creep of the C-S-H particles themselves, evolutions of the viscoelastic Poisson's ratio observed experimentally cannot be explained if one considers that the C-S-H particles are spherical and that they creep by sliding of its C-S-H layers over each other: either the C-S-H particles need to be considered aspherical, or the interlayer distance between neighboring C-S-H layers must be considered to vary in the long term.

5.2.2. Creep of C-S-H gel originating from creep of contact points between neighboring C-S-H particles

In this section, we consider that creep of the C-S-H gel originates from creep of the contact points between C-S-H particles, and that C-S-H particles only deform elastically.

Maalej [59] developed an elastic homogenization scheme for a composite material made of rigid spherical particles in contact through elastic contact points: to those contact points are associated a normal stiffness K_n and a tangential stiffness K_t (see Fig. 8b). In order to predict the viscoelastic behavior of the C-S-H gel here considered, in which contact points are considered viscoelastic, we extend Maalej's scheme to homogenization of the long-term viscoelastic behavior, again by using the correspondence principle and the final value theorem [42]. Thus, we obtain a relationship between the long-term viscoelastic Poisson's ratio ν_{gel}^{∞} of the C-S-H gel, its porosity, the long-term asymptotic values K_n^{∞} of the normal stiffness and K_t^{∞} of the tangential stiffness.

For spherical C-S-H particles and a gel porosity equal to 0.28, the long-term viscoelastic Poisson's ratio ν_{gel}^{∞} of the C-S-H gel is displayed in Fig. 9b as a function of the ratio $K_t^{\infty}/K_n^{\infty}$. If C-S-H particles can only slide over each other, i.e., if $K_t^{\infty}/K_n^{\infty} = 0$, the long-term

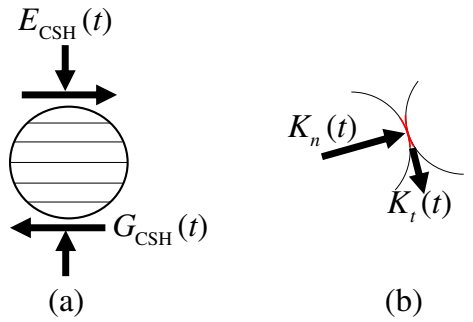

Fig. 8. (a) Layered structure of C-S-H particles. (b) Viscoelastic contact between C-S-H particles.

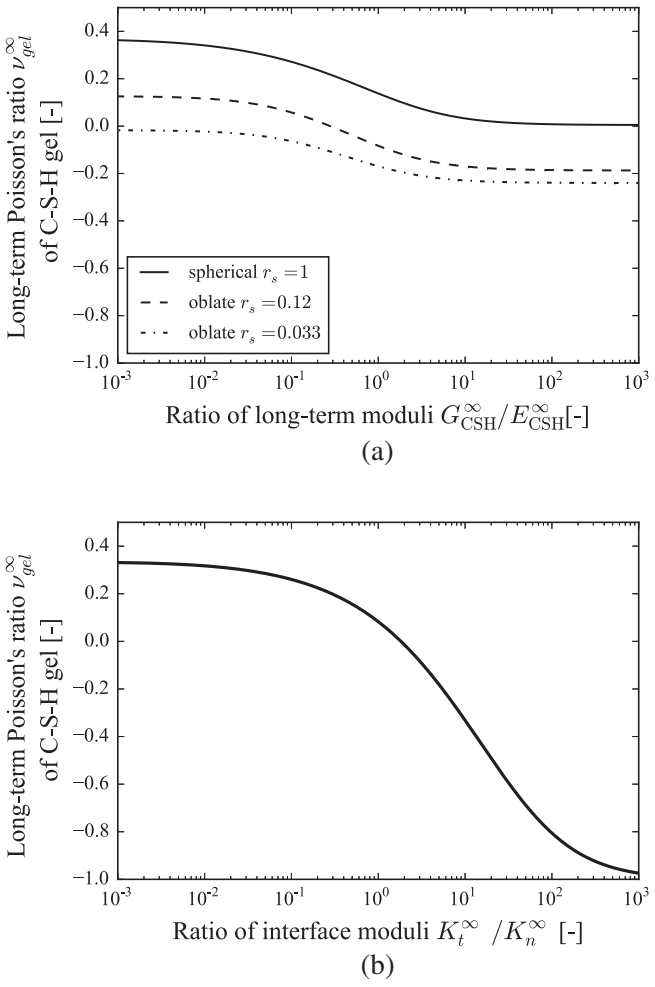

Fig. 9. Long-term viscoelastic Poisson's ratio ν_{gel}^{∞} of C-S-H gel: (a) in the case where creep is due to creep of the C-S-H particles themselves, and (b) in the case where creep is due to creep of contact points between neighboring C-S-H particles.

viscoelastic Poisson's ratio of the C-S-H gel is predicted to be equal to 0.33, which is greater than the values observed experimentally, which lay between −0.07 and 0.16 (see Fig. 6). Therefore, if creep of the C-S-H gel originates from the creep of the contact points between C-S-H particles, if one considers that C-S-H particles are spherical, he/she cannot consider that C-S-H particles can only slide over each other: in the long term, the C-S-H particles must also be allowed to get closer to each other, i.e., to interpenetrate each other.

We found no homogenization scheme that predicts the elastic behavior of an assembly of rigid particles in contact through elastic contact points, when the particles are considered aspherical. Therefore, we do not know how the conclusions drawn in this section would hold if the assumption of sphericity of the C-S-H particles was relaxed. However, given the results obtained in Section 5.2.1, conclusions are likely to significantly differ for aspherical particles. This elastic homogenization problem is difficult from a technical point of view. As a starting point, Sidhom [60] proposed some bounds on the effective moduli, using energy approaches, but these bounds may not be tight enough to be directly applied to this study.

6. Conclusions

We analyzed the long-term viscoelastic Poisson's ratio of concrete from creep experiments from the literature. The results were used to compute the long-term viscoelastic Poisson's ratio of C-S-H gel by downscaling with the help of elastic homogenization schemes extended to viscoelasticity. Several conclusions can be drawn.

For what concerns creep of concrete, the analysis of all experimental results shows that:

- The time-dependent behavior of concrete is isotropic, as expected from the theory of linear viscoelasticity.
- The long-term creep of concrete is not only deviatoric, but also volumetric.
- The long-term viscoelastic Poisson's ratio of concrete is equal to or smaller than its elastic Poisson's ratio, and comprised between 0.15 and 0.20.
- When the elastic Poisson's ratio of mature concrete is significantly greater than 0.20, the variation of its viscoelastic Poisson's ratio over time is non-negligible.
- When the elastic Poisson's ratio of mature concrete is comprised between 0.15 and 0.20, for practical applications, considering that its viscoelastic Poisson's ratio is constant over time, as proposed in particular by Bažant [2,40], is a very reasonable assumption.

For what concerns downscaling of the viscoelastic Poisson's ratio of concrete, if the aggregates, portlandite, calcium sulfoaluminates hydrates and clinker can be considered as spherical:

- The long-term viscoelastic Poisson's ratio of the C-S-H gel has little effect on the long-term viscoelastic Poisson's ratio of concrete.
- The interface between aggregates and cement paste can be considered adhesive for downscaling or upscaling the long-term viscoelastic Poisson's ratio.
- The interface between portlandite, calcium sulfoaluminates hydrates and clinker on one hand, and the mixture of C-S-H with the capillary porosity on the other hand, has little effect on the relation between the viscoelastic Poisson's ratio of concrete and that of the C-S-H gel.

For what concerns creep of the C-S-H gel, if we consider that the experimental data at the concrete scale are sufficiently reliable, downscaling of all experimental results obtained at the scale of concrete shows that:

- The long-term viscoelastic Poisson's ratio of the C-S-H gel is comprised between 0 and 0.2.
- The long-term creep of C-S-H gel in concrete is both deviatoric and volumetric.
- If creep of the C-S-H gel is due to creep of the C-S-H particles themselves, evolutions of the creep Poisson's ratio observed experimentally cannot be explained if one considers that the C-S-H particles are spherical and that they creep by sliding of its C-S-H layers over each other: either the C-S-H particles need to be considered aspherical, or the interlayer distance between neighboring C-S-H layers must be considered to vary in the long term.
- If creep of the C-S-H gel is due to creep of the contact points between C-S-H particles, and if one considers that C-S-H particles are spherical, he/she cannot consider that C-S-H particles can only slide over each other: in the long term, the C-S-H particles must also be allowed to get closer to each other, i.e., to interpenetrate each other.

Acknowledgements

The authors acknowledge financial support from EDF (grant number: 3000-4310005728) and thank EDF for this support.

Appendix A. Comparaison of Poisson's ratio and creep-based Poisson's ratio in different directions

In this section, for the 11 tests in [22], we computed the 3 directional creep-based Poisson's ratios with Eq. 11 (as did the authors) and the 3 directional creep-based Poisson's ratios with Eqs. (5a) and (5b) . The results are plotted in Figs. A.10–A.13.

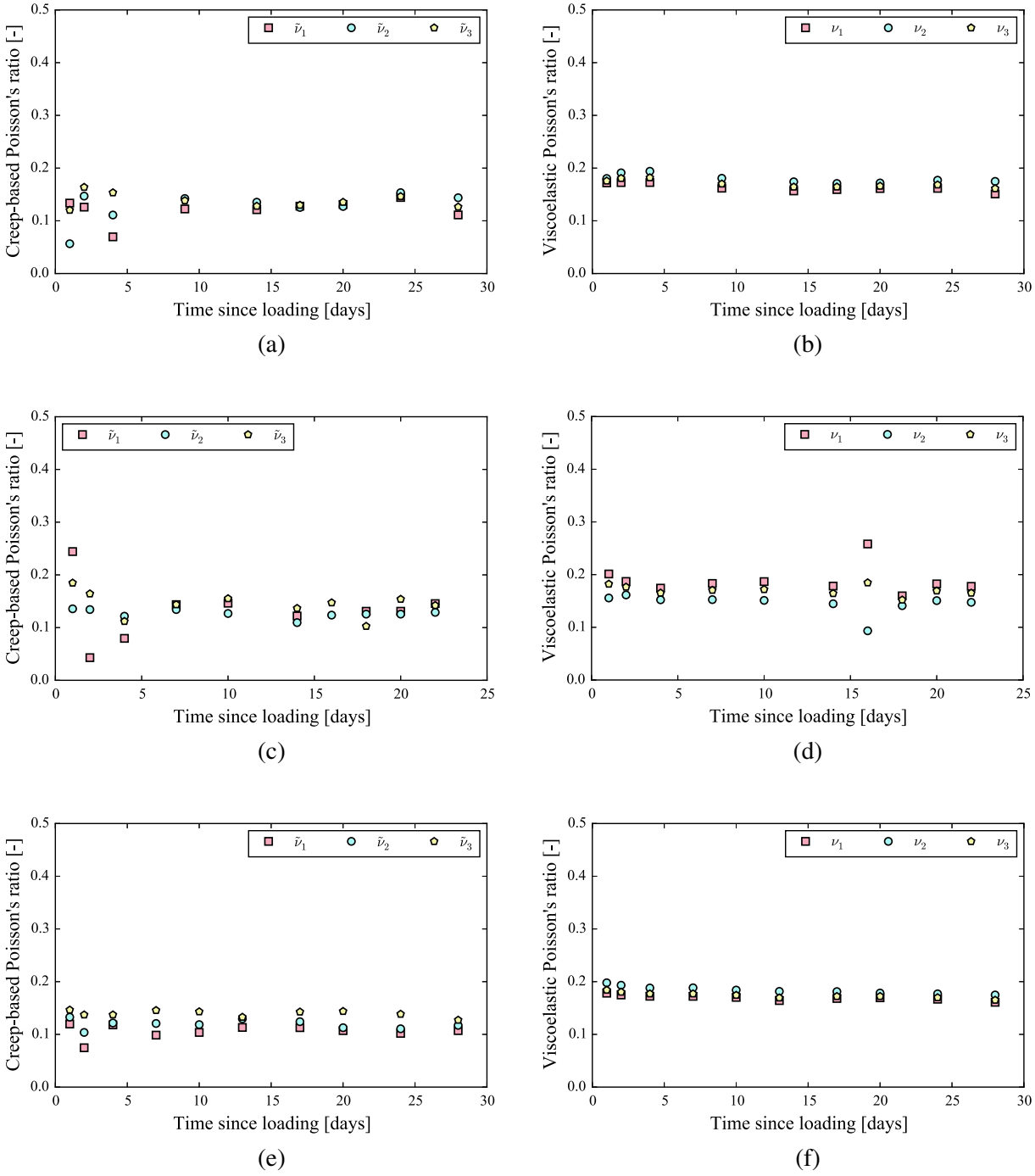

Fig. A.10. Dependency of Poisson's ratio on the direction: (a), (c) and (e) creep-based Poisson's ratio reported in [22], calculated from Eq. (11) for three directions; (b), (d) and (f) viscoelastic Poisson's ratio calculated from Eqs. (5a) and (5b) for three directions. Data (a) and (b) from experiment TC1, (c) and (d) from experiment BC4and (e) and (f) from experiment TC5 in [22].

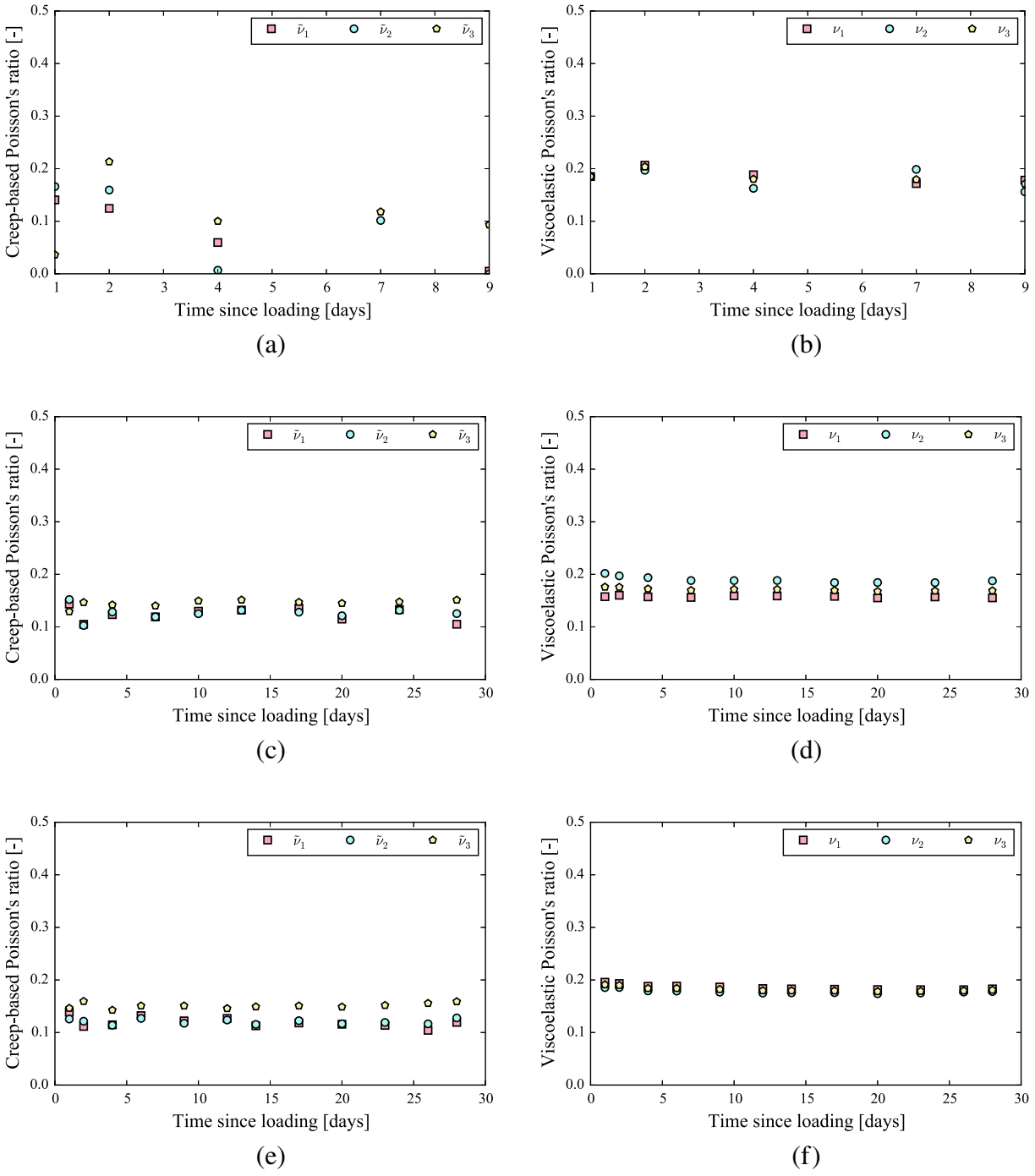

Fig. A.11. Dependency of Poisson's ratio on the direction: (a), (c) and (e) creep-based Poisson's ratio reported in [22], calculated from Eq. (11) for three directions; (b), (d) and (f) viscoelastic Poisson's ratio calculated from Eqs. (5a) and (5b) for three directions. Data (a) and (b) from experiment TC5R, (c) and (d) from experiment TC6and (e) and (f) from experiment TC7 in [22].

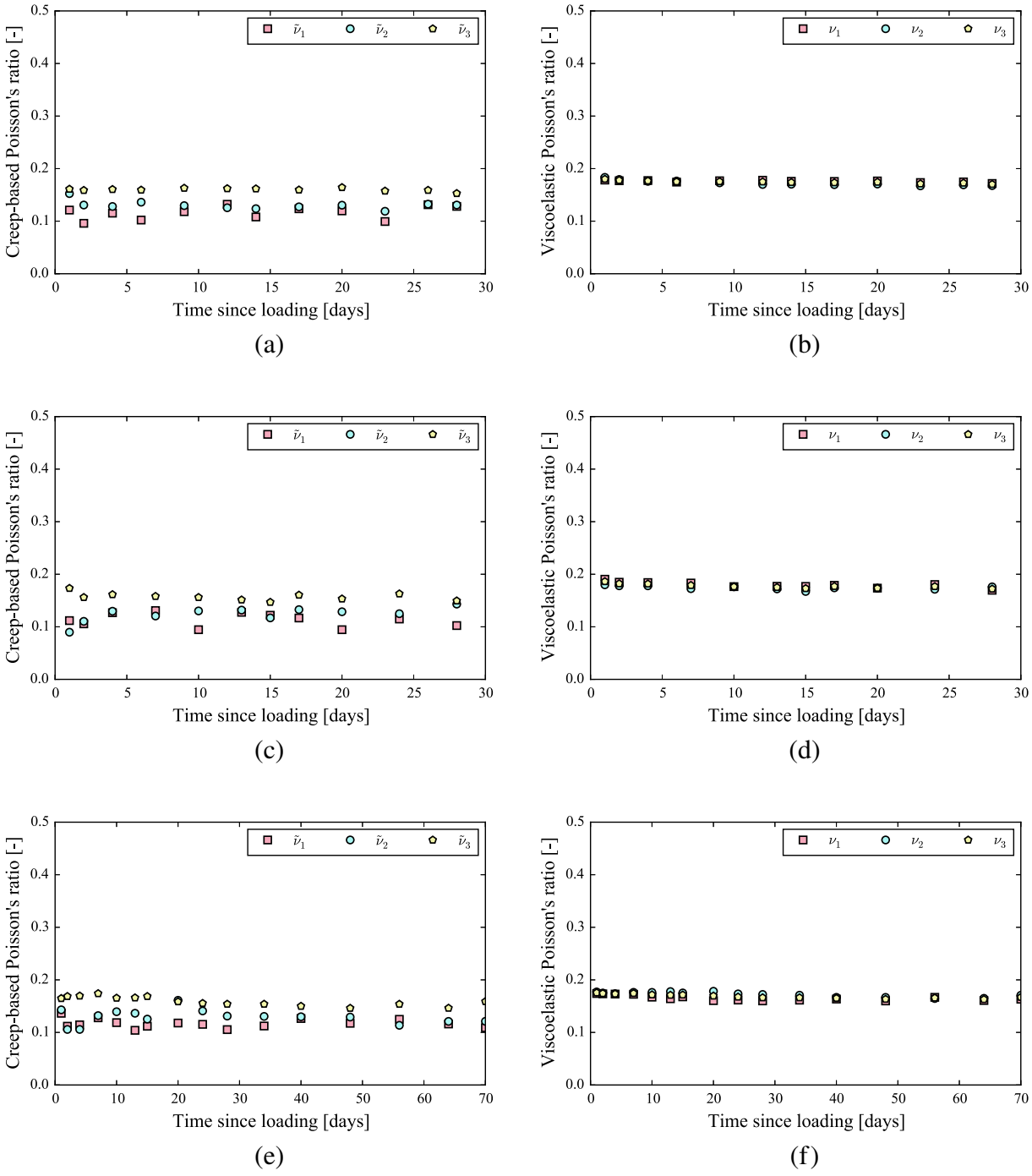

Fig. A.12. Dependency of Poisson's ratio on the direction: (a), (c) and (e) creep-based Poisson's ratio reported in [22], calculated from Eq. (11) for three directions; (b), (d) and (f) viscoelastic Poisson's ratio calculated from Eqs. (5a) and (5b) for three directions. Data (a) and (b) from experiment BC8, (c) and (d) from experiment BT9and (e) and (f) from experiment TC11 in [22].

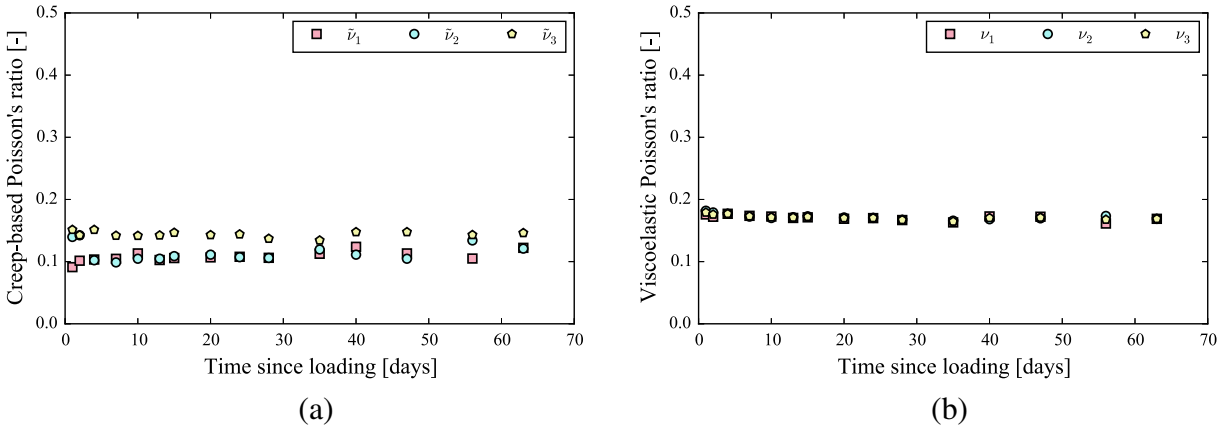

Fig. A.13. Dependency of Poisson's ratio on the direction in experiment TC12 in [22]: (a) creep-based Poisson's ratio reported in [22], calculated from Eq. (11) for three directions; (b) viscoelastic Poisson's ratio calculated from Eqs. (5a) and (5b) for three directions.

Appendix B. Experimental data of concrete Poisson's ratio from literature

In this section, we present all the experimental data of the evolution of Poisson's ratio of concrete. The evolution of the Poisson's ratio is computed from Eqs. (5a) and (5b). Each test is described briefly in the following:

Gopalakrishnan's[22] tests are on cubic sample concrete. The load is applied at the age of 8 days in three direction consequently. The values of load are:

- Test TC1: $\sigma_1 = -5.69$ MPa, $\sigma_2 = -5.55$ MPa, $\sigma_3 = -3.59$ MPa;
- Test BC4: $\sigma_1 = -5.21$ MPa, $\sigma_2 = -3.59$ MPa, $\sigma_3 = -0$;
- Test TC5: $\sigma_1 = -10.0$ MPa, $\sigma_2 = -7.72$ MPa, $\sigma_3 = -3.14$ MPa;
- Test TC5R: $\sigma_1 = -9.89$ MPa, $\sigma_2 = -7.55$ MPa, $\sigma_3 = -3.03$ MPa;
- Test TC6: $\sigma_1 = -11.2$ MPa, $\sigma_2 = -9.72$ MPa, $\sigma_3 = -2.10$ MPa;
- Test TC7: $\sigma_1 = -12.55$ MPa, $\sigma_2 = -11.45$ MPa, $\sigma_3 = -2.45$ MPa;
- Test BC8: $\sigma_1 = -12.58$ MPa, $\sigma_2 = -7.24$ MPa, $\sigma_3 = 0$;
- Test BT9: $\sigma_1 = -8.41$ MPa, $\sigma_2 = -5.62$ MPa, $\sigma_3 = 0$;
- Test TC10: $\sigma_1 = -13.24$ MPa, $\sigma_2 = -1.76$ MPa, $\sigma_3 = -1.83$ MPa;
- Test BT11: $\sigma_1 = -13.38$ MPa, $\sigma_2 = -13.89$ MPa, $\sigma_3 = 0$;
- Test TC12: $\sigma_1 = -12.82$ MPa, $\sigma_2 = -13.24$ MPa, $\sigma_3 = -6.34$ MPa;

The evolution of Poisson's ratio in these test are displayed in Fig. B.1.

Jordaan et Illston [9,18] tested cubic sample of concrete under uniaxial and biaxial load. Loading age is 16 days. The load values for the tests from [9] are:

- Serie 1, uniaxial test: $\sigma_1 = -10.0$ MPa, $\sigma_2 = \sigma_3 = 0$;
- Serie 1, biaxial test: $\sigma_1 = \sigma_2 = -9.50$ MPa, $\sigma_3 = 0$;
- Serie 2, uniaxial test: $\sigma_1 = -10.6$ MPa, $\sigma_2 = \sigma_3 = 0$;
- Serie 2, biaxial test: $\sigma_1 = -10.6$ MPa, $\sigma_2 = -3.32$ MPa, $\sigma_3 = 0$;

The load values for the tests from [18] are:

- Uniaxial test: $\sigma_1 = -5.2$ MPa, $\sigma_2 = \sigma_3 = 0$;
- Biaxial test: $\sigma_1 = -5.2$ MPa, $\sigma_2 = -6.9$ MPa, $\sigma_3 = 0$;
- Triaxial test: $\sigma_1 = -5.2$ MPa, $\sigma_2 = -6.9$ MPa, $\sigma_3 = 3.5$ MPa;

The evolution of Poisson's ratio for the test from [9] are displayed in Fig. B.2a and those from [18] are displayed in Fig. B.2b.

Kennedy [19] performed uniaxial and triaxial creep tests on cyclindrical specimen. The axial load σ_a and radial load σ_r are list in the following list, as well as loading age:

- As-Cast, B7: $\sigma_a = -16.55$ MPa, $\sigma_r = 0$, loading age 90 days;
- As-Cast, C23: $\sigma_a = 0$, $\sigma_r = -16.55$ MPa, loading age 90 days;
- As-Cast, E39: $\sigma_a = 4.14$ MPa, $\sigma_r = 0$, loading age 90 days;
- As-Cast, F13: $\sigma_a = 0$, $\sigma_r = -4.14$ MPa, loading age 90 days;
- As-Cast, G35: $\sigma_a = -4.14$ MPa, $\sigma_r = -24.82$ MPa, loading age 90 days;
- As-Cast, H5: $\sigma_a = -4.14$ MPa, $\sigma_r = 0$, loading age 365 days;
- As-Cast, H22: $\sigma_a = 0$, $\sigma_r = -24.82$ MPa, loading age 90 days;
- As-Cast, H24: $\sigma_a = -16.55$ MPa, $\sigma_r = 0$, loading age 365 days;
- As-Cast, H34: $\sigma_a = -16.55$ MPa, $\sigma_r = 0$, loading age 183 days;
- As-Cast, H45: $\sigma_a = -4.14$ MPa, $\sigma_r = 0$, loading age 183 days;

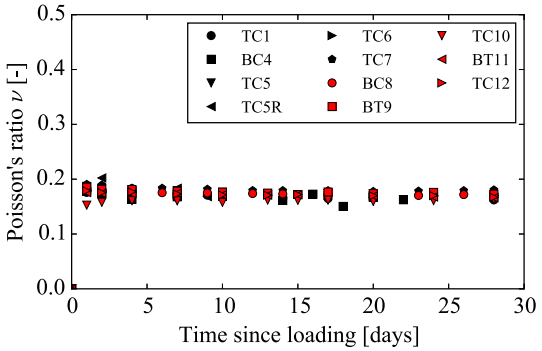

Fig. B.1. Poisson's ratio of concrete versus time. Data retrieved from [22].

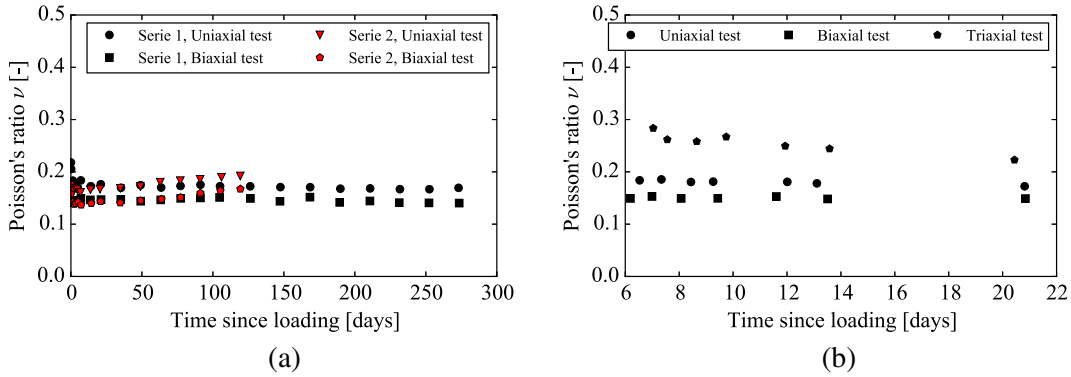

Fig. B.2. (a) Poisson's ratio versus time. Data retrieved from [9]. (b) Poisson's ratio versus time. Data retrieved from [18].

- Air-Dried, B19: $\sigma_a = -16.55$ MPa, $\sigma_r = 0$, loading age 90 days;
- Air-Dried, E40: $\sigma_a = 4.14$ MPa, $\sigma_r = 0$, loading age 90 days;
- Air-Dried, G30: $\sigma_a = -4.14$ MPa, $\sigma_r = -24.82$ MPa, loading age 90 days;
- Air-Dried, H17: $\sigma_a = -16.55$ MPa, $\sigma_r = 0$, loading age 365 days;
- Air-Dried, H31: $\sigma_a = -4.14$ MPa, $\sigma_r = 0$, loading age 365 days;
- Air-Dried, I20: $\sigma_a = -16.55$ MPa, $\sigma_r = 0$, loading age 183 days;
- Air-Dried, I39: $\sigma_a = -4.14$ MPa, $\sigma_r = 0$, loading age 183 days;

The evolution of the Poisson's ratio for As-Cast samples are displayed in Fig. B.3a and those for Air-Dried samples are displayed in Fig. B.3b.

Kim et al.[21] tested cubic concrete sample which are cured until age of 28 days under water. The loading age is 28 days. The load values for each test are:

- Concrete C1, uniaxial test 1: $\sigma_1 = -4.90$ MPa, $\sigma_2 = \sigma_3 = 0$;
- Concrete C1, uniaxial test 2: $\sigma_1 = -9.80$ MPa, $\sigma_2 = \sigma_3 = 0$;
- Concrete C1, biaxial test 1: $\sigma_1 = -4.90$ MPa, $\sigma_2 = -0.98$ MPa, $\sigma_3 = 0$;
- Concrete C1, biaxial test 2: $\sigma_1 = -4.90$ MPa, $\sigma_2 = -1.96$ MPa, $\sigma_3 = 0$;
- Concrete C1, biaxial test 3: $\sigma_1 = -9.80$ MPa, $\sigma_2 = -1.96$ MPa, $\sigma_3 = 0$;
- Concrete C1, triaxial test 1: $\sigma_1 = -4.90$ MPa, $\sigma_2 = \sigma_3 = -0.49$ MPa;
- Concrete C1, triaxial test 2: $\sigma_1 = -4.90$ MPa, $\sigma_2 = \sigma_3 = -0.98$ MPa;
- Concrete C1, triaxial test 3: $\sigma_1 = -4.90$ MPa, $\sigma_2 = \sigma_3 = -1.96$ MPa;
- Concrete C1, triaxial test 4: $\sigma_1 = -4.90$ MPa, $\sigma_2 = -1.96$ MPa, $\sigma_3 = -0.98$ MPa;
- Concrete C2, uniaxial test 1: $\sigma_1 = -7.35$ MPa, $\sigma_2 = \sigma_3 = 0$;
- Concrete C2, uniaxial test 2: $\sigma_1 = -9.80$ MPa, $\sigma_2 = \sigma_3 = 0$;
- Concrete C2, biaxial test 1: $\sigma_1 = -7.35$ MPa, $\sigma_2 = -1.47$ MPa, $\sigma_3 = 0$;
- Concrete C2, biaxial test 2: $\sigma_1 = -7.35$ MPa, $\sigma_2 = -2.94$ MPa, $\sigma_3 = 0$;
- Concrete C2, biaxial test 3: $\sigma_1 = -9.80$ MPa, $\sigma_2 = -2.94$ MPa, $\sigma_3 = 0$;
- Concrete C2, triaxial test 1: $\sigma_1 = -7.35$ MPa, $\sigma_2 = \sigma_3 = -0.74$ MPa;
- Concrete C2, triaxial test 2: $\sigma_1 = -7.35$ MPa, $\sigma_2 = \sigma_3 = -1.47$ MPa;
- Concrete C2, triaxial test 3: $\sigma_1 = -7.35$ MPa, $\sigma_2 = \sigma_3 = -2.94$ MPa;
- Concrete C2, triaxial test 4: $\sigma_1 = -7.35$ MPa, $\sigma_2 = -2.94$ MPa, $\sigma_3 = -1.96$ MPa;
- Concrete C3, uniaxial test 1: $\sigma_1 = -9.80$ MPa, $\sigma_2 = \sigma_3 = 0$;
- Concrete C3, uniaxial test 2: $\sigma_1 = -12.25$ MPa, $\sigma_2 = \sigma_3 = 0$;

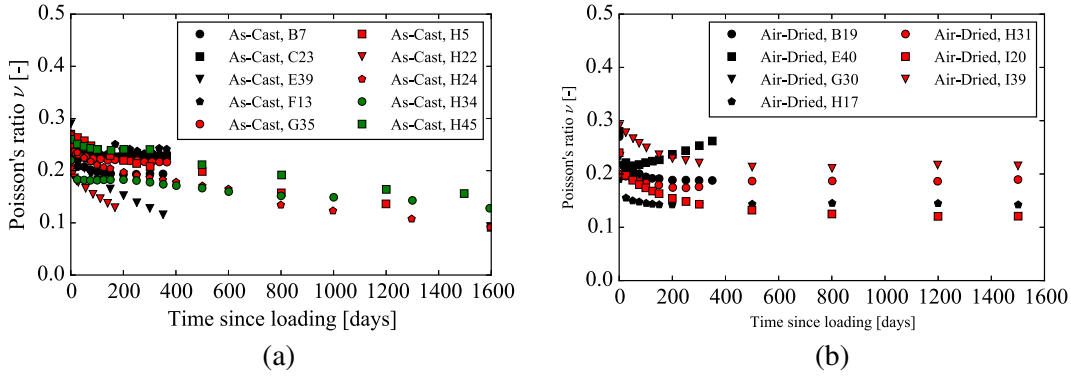

Fig. B.3. (a) Poisson's ratio versus time for As-Cast concrete specimens. Data retrieved from [19]. (b) Poisson's ratio versus time for Air-Dried specimens. Data retrieved from [19].

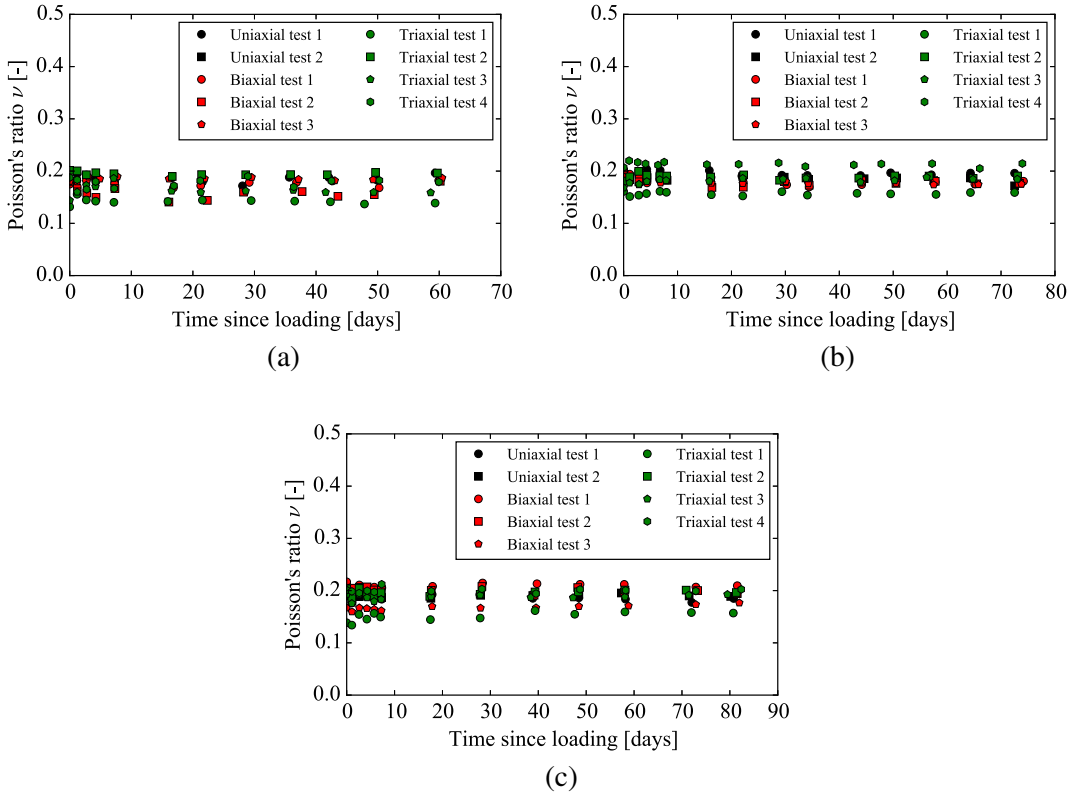

Fig. B.4. (a) Poisson's ratio versus time for C1 concrete specimens. Data retrieved from [21]. (b) Poisson's ratio versus time for C2 concrete specimens. Data retrieved from [21]. (c) Poisson's ratio versus time for C3 concrete specimens. Data retrieved from [21].

- Concrete C3, biaxial test 1: $\sigma_1 = -9.80$ MPa, $\sigma_2 = -1.96$ MPa, $\sigma_3 = 0$;
- Concrete C3, biaxial test 2: $\sigma_1 = -9.80$ MPa, $\sigma_2 = -3.92$ MPa, $\sigma_3 = 0$;
- Concrete C3, biaxial test 3: $\sigma_1 = -12.25$ MPa, $\sigma_2 = -3.92$ MPa, $\sigma_3 = 0$;
- Concrete C3, triaxial test 1: $\sigma_1 = -9.80$ MPa, $\sigma_2 = \sigma_3 = -0.98$ MPa;
- Concrete C3, triaxial test 2: $\sigma_1 = -9.80$ MPa, $\sigma_2 = \sigma_3 = -1.96$ MPa;
- Concrete C3, triaxial test 3: $\sigma_1 = -9.80$ MPa, $\sigma_2 = \sigma_3 = -3.92$ MPa;
- Concrete C3, triaxial test 4: $\sigma_1 = -9.80$ MPa, $\sigma_2 = -3.92$ MPa, $\sigma_3 = -1.96$ MPa;

The evolution of Poisson's ratio for concrete C1, C2 and C3 are displayed in Fig. B.4a, b and c, respectively.

References

[1] J.-M. Torrenti, F. Benboudjema, F. Barré, E. Gallitre, On the very long term delayed behaviour of concrete, Proceedings of the International Conference on Ageing of Materials & Structures, 2014, 218885.
[2] RILEM Technical Committee, Creep and shrinkage prediction model for analysis and design of concrete structures-model B3, Mater. Struct. 28 (1995) 357–365.
[3] RILEM Technical Committee, RILEM Draft recommendation: TC-242-MDC multi-decade creep and shrinkage of concrete: material model and structural analysis, Mater. Struct. 48 (4) (2015) 753–770. http://link.springer.com/10.1617/s11527-014-0485-2. http://dx.doi.org/10.1617/s11527-014-0485-2.
[4] fib, Model code for concrete structures 2010, Ernst and Son. 2013,
[5] E. 1992-1-1:2005, Eurocode 2: design of concrete structures: part 1-1: general rules and rules for buildings, CEN.
[6] ACI Committee 209, Guide for modeling and calculating shrinkage and creep in hardened concrete (ACI 209.2R-08), American Concrete Institute. 2008,
[7] A. Aili, M. Vandamme, J.-M. Torrenti, B. Masson, Theoretical and practical differences between creep and relaxation Poisson's ratios in linear viscoelasticity, Mech. Time-Depend. Mater. 19 (4) (2015) 537–555. http://dx.doi.org/10.1007/s11043-015-9277-5.
[8] A.M. Neville, W.H. Dilger, J.J. Brooks, Creep of Plain and Structural Concrete, Construction Press. 1983.
[9] I.J. Jordaan, J.M. Illston, The creep of sealed concrete under multiaxial compressive stresses, Mag. Concr. Res. 21 (69) (1969) 195–204.
[10] A. Ross, Experiments on the creep of concrete under two-dimensional stressing, Mag. Concr. Res. 6 (16) (1954) 3–10.
[11] H.L. Furr, Creep tests of two-way prestressed concrete,ACI Journal Proceedings, vol. 64, ACI. 1967,
[12] W. Glanville, F. Thomas, Studies in reinforced concrete: further investigations on the creep or flow of concrete under load. IV, Building Research Technical Paper No. 21, London, 1939,
[13] R. L'Hermite, What do we know about the plastic deformation and creep of concrete, RILEM Bulletin, No. 1, Paris, 1959, pp. 888–896.
[14] C.M. Duke, H.E. Davis, Some properties of concrete under sustained combined stresses, ASTM Proc. 44 (1944) 888–896.
[15] M. Polivka, D. Pirtz, R.F. Adams, Studies of creep in mass concrete, ACI Spec. Publ. 6 (1963) 257–283.
[16] R.H. Evans, R.H. Wood, Transverse elasticity of building materials, Engineering 143 (1937) 161–163.
[17] G.P. York, T.W. Kennedy, E.S. Perry, J.N. Thompson, Experimental determination of Poisson's ratio for creep, ACI J. Spec. Publ. 34 (1972) 535–546.
[18] I.J. Jordaan, J.M. Illston, Time dependent strains in sealed concrete under systems of variable multiaxial stress, Mag. Concr. Res. 23 (75-76) (1971) 79–88.
[19] T.W. Kennedy, An evolution and summary of a study of the long-term multiaxial creep behavior of concrete, Tech. Rep., Oak Ridge National Laboratory. 1975,
[20] F.-J. Ulm, F. Le Maou, C. Boulay, Creep and shrinkage of concrete-kinetics approach, ACI Spec. Publ. 194 (2000) 135–153.
[21] J.K. Kim, S.H. Kwon, S.Y. Kim, Y.Y. Kim, Experimental studies on creep of sealed concrete under multiaxial stresses, Mag. Concr. Res. 57 (10) (2005) 623–634.
[22] K.S. Gopalakrishnan, Creep of Concrete under Multiaxial Compressive Stresses, Civil Engineering, University of Calgary. 1968, (Ph.D. thesis). http://dhl.handle.net/1880/1815.
[23] P.K. Mehta, P.J. Monteiro, Concrete: Microstructure, Properties, and Materials, 3rd edition ed., McGraw-Hill, New York, 2006.
[24] Z.C. Grasley, D.A. Lange, Constitutive modeling of the aging viscoelastic properties of Portland cement paste, Mech. Time-Depend. Mater. 11 (3) (2007) 175–198. http://dx.doi.org/10.1007/s11043-007-9043-4.

[25] X. Li, Z. Grasley, J. Bullard, E. Garboczi, Computing the time evolution of the apparent viscoelastic/viscoplastic Poisson's ratio of hydrating cement paste, Cem. Concr. Compos. 56 (2015) 121–133. http://www.sciencedirect.com/science/article/pii/S0958946514002078. http://dx.doi.org/10.1016/j.cemconcomp.2014.11.004.
[26] R. Christensen, Theory of Viscoelasticity: An Introduction, Elsevier. 1982.
[27] Z.P. Bažant, Y.-P. Xi, S. Baweja, I. Carol, Preliminary guidelines and recommendation for characterizing creep and shrinkage in structural design codes, RILEM Proceedings, CHAPMAN & HALL. 1993, 805–805.
[28] H.H. Hilton, Implications and constraints of time-independent Poisson ratios in linear isotropic and anisotropic viscoelasticity, J. Elast. 63 (2001) 221–251.
[29] N.W. Tschoegl, W.G. Knauss, I. Emri, Poisson's ratio in linear viscoelasticity - a critical review, Mech. Time-Depend. Mater. 7 (6) (2002) 3–51. http://dx.doi.org/10.1023/A:1014411503 17.
[30] H.H. Hilton, The elusive and fickle viscoelastic Poisson's ratio and its relation to the elastic-viscoelastic corresponding principle, J. Mech. Mater. Struct. 4 (September) (2009) 1341–1364.
[31] H.H. Hilton, Clarifications of certain ambiguities and failings of Poisson's ratios in linear viscoelasticity, J. Elast. 104 (1-2) (2011) 303–318. http://link.springer.com/10.1007/s10659-010-9296-z. http://dx.doi.org/10.1007/s10659-010-9296-z.
[32] K.S. Gopalakrishnan, A.M. Neville, A. Ghali, Creep Poisson's ratio of concrete under multiaxial compression, ACI J. 66 (66) (1969) 1008–1020.
[33] O. Bernard, F.-J. Ulm, J.T. Germaine, Volume and deviator creep of calcium-leached cement-based materials, Cem. Concr. Res. 33 (8) (2003) 1127–1136. http://linkinghub.elsevier.com/retrieve/pii/S0008884603000218.
[34] D. Hannant, Strain behaviour of concrete up to 95 °C under compressive stresses, Proc. Conference on Prestressed Concrete Pressure Vessels Group C, Institution of Civil Engineers, London, 1967, pp. 57–71.
[35] E.A. Kogan, Creep of concrete under multiaxial compression, Hydrotech. Constr. 17 (9) (1983) 448–452.
[36] L. Granger, Comportement différé du béton dans les enceintes de centrales nucléaires: analyse et modélisation, Ecole Nationale des Ponts et Chaussées. 1995. (Ph.D. thesis)
[37] Z.P. Bažant, A.B. Hauggaard, S. Baweja, F.-J. Ulm, Microprestress-solidification theory for concrete creep. i: aging and drying effects, J. Eng. Mech. 123 (11) (1997) 1188–1194.
[38] F. Benboudjema, Modélisation des déformations différées du béton sous sollicitations biaxiales. Application aux enceintes de confinement de bâtiments réacteurs des centrales nucléaires, Université de Marne-la-Vallée. 2002. (Ph.D. thesis)
[39] A. Hilaire, étude des déformations différées des bétons en compression et en traction, du jeune âge au long terme, École Normale Supérieure de Cachan. 2014. (Ph.D. thesis)
[40] Z.P. Bažant, Theory of creep and shrinkage in concrete structures: a precis of recent developments, Mech. Today 2 (1975) 1–93.
[41] L. Parrott, Lateral strains in hardened cement paste under short-and long-term loading, Mag. Concr. Res. 26 (89) (1974) 198–202.
[42] G. Auliac, J. Avignant, É. Azoulay, Techniques Mathématiques Pour La Physique, Ellipses. 2000.
[43] Z.P. Bažant, M.H. Hubler, Q. Yu, Pervasiveness of excessive segmental bridge deflections: wake-up call for creep, ACI Struct. J. 108 (6) (2011) 766.
[44] H.S. Müller, I. Anders, R. Breiner, M. Vogel, Concrete: treatment of types and properties in fib model code 2010, Struct. Concr. 14 (4) (2013) 320–334. http://dx.doi.org/10.1002/suco.201200048.
[45] J.-M. Torrenti, R. Le Roy, Analysis and modelling of basic creep, CONCREEP 10, American Society of Civil Engineers, Reston, VA, 2015, pp. 1400–1409. http://ascelibrary.org/doi/10.1061/9780784479346.165. http://dx.doi.org/10.1061/9780784479346.165.
[46] J. Sanahuja, Effective behaviour of ageing linear viscoelastic composites: homogenization approach, Int. J. Solids Struct. 50 (19) (2013) 2846–2856. http://www.sciencedirect.com/science/article/pii/S0020768313001807. http://dx.doi.org/10.1016/j.ijsolstr.2013.04.023.
[47] O. Bernard, F.-J. Ulm, E. Lemarchand, A multiscale micromechanics-hydration model for the early-age elastic properties of cement-based materials, Cem. Concr. Res. 33 (9) (2003) 1293–1309. http://www.sciencedirect.com/science/article/pii/S0008884603000395. http://dx.doi.org/10.1016/S0008-8846(03)00039-5.
[48] J. Sanahuja, L. Dormieux, G. Chanvillard, Modelling elasticity of a hydrating cement paste, Cem. Concr. Res. 37 (10) (2007) 1427–1439. http://www.sciencedirect.com/science/article/pii/S0008884607001548. http://dx.doi.org/10.1016/j.cemconres.2007.07.003.
[49] B. Pichler, C. Hellmich, Upscaling quasi-brittle strength of cement paste and mortar: a multi-scale engineering mechanics model, Cem. Concr. Res. 41 (5) (2011) 467–476. http://www.sciencedirect.com/science/article/pii/S0008884611000111. http://dx.doi.org/10.1016/j.cemconres.2011.01.010.
[50] R. Le Roy, Déformations instantanées et différées des bétons à hautes performances, École Nationale des Ponts et Chaussées. 1995. (Ph.D. thesis)
[51] Q. Zhang, R.L. Roy, M. Vandamme, B. Zuber, Long-term creep properties of cementitious materials: comparing microindentation testing with macroscopic uniaxial compressive testing, Cem. Concr. Res. 58 (2014) 89–98. http://www.sciencedirect.com/science/article/pii/S0008884614000052. http://dx.doi.org/10.1016/j.cemconres.2014.01.004.
[52] H.F. Taylor, Cement Chemistry, Thomas Telford. 1997.
[53] H. Duan, X. Yi, Z. Huang, J. Wang, A unified scheme for prediction of effective moduli of multiphase composites with interface effects. Part I: theoretical framework, Mech. Mater. 39 (1) (2007) 81–93.
[54] J.-F. Barthélémy, Approche micromécanique de la rupture et de la fissuration dans les géomatériaux, École Nationale des Ponts et Chaussées. 2005, (Ph.D. thesis). http://www.theses.fr/2005ENPC0006.
[55] H.M. Jennings, A model for the microstructure of calcium silicate hydrate in cement paste, Cem. Concr. Res. 30 (1) (2000) 101–116. http://www.sciencedirect.com/science/article/pii/S0008884699002094. http://dx.doi.org/10.1016/S0008-8846(99)00209-4.
[56] H.M. Jennings, Colloid model of C-S-H and implications to the problem of creep and shrinkage, Mater. Struct. 37 (1) (2004) 59–70. http://dx.doi.org/10.1007/BF02481627.
[57] P.D. Tennis, H.M. Jennings, A model for two types of calcium silicate hydrate in the microstructure of Portland cement pastes, Cem. Concr. Res. 30 (6) (2000) 855–863. http://www.sciencedirect.com/science/article/pii/S000884600000257X. http://dx.doi.org/10.1016/S0008-8846(00)00257-X.
[58] J. Sanahuja, Impact de la morphologie structurale sur les performances mécaniques des matériaux de construction : application au plâtre et à la pâte de ciment, École Normale Supérieure de Cachan. 2008, (Ph.D. thesis). http://www.theses.fr/2008ENPC0808.
[59] Y. Maalej, Mechanical Behaviour of a Grouted Granular Medium : Experimental Study and Micromechanical Modelization, Ecole Nationale des Ponts et Chaussées. 2007, (Ph.D. thesis). https://pastel.archives-ouvertes.fr/tel-00141156.
[60] M. Sidhom, Multi-scale Approaches of Granular Composites with Interface Effects : Application to Nanocomposites and Cement Based Composites, Université Paris-Est. 2014, (Ph.D. thesis). https://pastel.archives-ouvertes.fr/tel-01167116.